12-9-2022

Quasi 1D modelling of a Scramjet engine cycle using Heiser-Pratt approach

Asmaa Chakir
mahchakir@gmail.com

Follow this and additional works at: https://scholarsjunction.msstate.edu/td

Part of the Aerodynamics and Fluid Mechanics Commons, and the Propulsion and Power Commons

Recommended Citation

Quasi 1D modelling of a Scramjet engine cycle using Heiser-Pratt approach

By

Asmaa Chakir

Approved by:

Shanti Bhushan (Major Professor)
Anup Zope
Eric Collins
Joonsik Hwang
Tonya W. Stone (Graduate Coordinator)
Jason M. Keith (Dean, Department of Mechanical Engineering)

A Thesis
Submitted to the Faculty of
Mississippi State University
in Partial Fulfillment of the Requirements
for the Master of Science
in Mechanical Engineering
in the Department of Mechanical Engineering

Mississippi State, Mississippi

December 2022

Name: Asmaa Chakir

Date of Degree: December 9, 2022

Institution: Mississippi State University

Major Field: Mechanical Engineering

Major Professor: Shanti Bhushan

Title of Study: Quasi 1D modelling of a Scramjet engine cycle using Heiser-Pratt approach

Pages in Study: 135

Candidate for Degree of Master of Science

Scramjet engines are key for sustained hypersonic flights. Analytic models play a critical role in the preliminary design of a scramjet engine configuration. The objective of this research is to develop and validate a quasi-1D model for the scramjet engine encompassing inlet, isolator and combustor, to evaluate the impact of flight conditions and design parameters on the engine functionality. The model is developed assuming isentropic flow in the inlet with a single turn; modified Fanno-flow equations in the isolator that account for the area change of the core flow; and the combustor is modeled using Heiser-Pratt equations accounting for the fuel mixing efficiency. The isolator and combustor models are validated against experimental results. The model accounts for twelve parameters allowing for a decent range of possible configurations. Finally, the model was applied to five sets of parametric studies to evaluate the effect of multiple parameters on the engine functionality.

DEDICATION

For my family: Dad, Mom, Rihab, Mossaab, and Mohammed.

ACKNOWLEDGEMENTS

TABLE OF CONTENTS

LIST OF TABLES

LIST OF FIGURES

CHAPTER I

INTRODUCTION

1.1   Airbreathing systems and the need of scramjet engine

Since the world wars, the competition in the aeronautical industry and notably in the propulsion systems has been accentuated. Many international efforts are deployed to target the different the various aspects of the field, such as: fuel consumption optimization, eco-friendly engines… One of the subjects that heavily attracts scientists and organizations is: "The hypersonic flight". Indeed, to keep pace with the speed of the modern world, the enormous progress in space-sailing, and demands of the military industry, producing faster mobility devices is a must. To accommodate this need, many air-breathing devices were invented. To mention but a few, the turbojets, the ramjets, the scramjets, and the rockets.
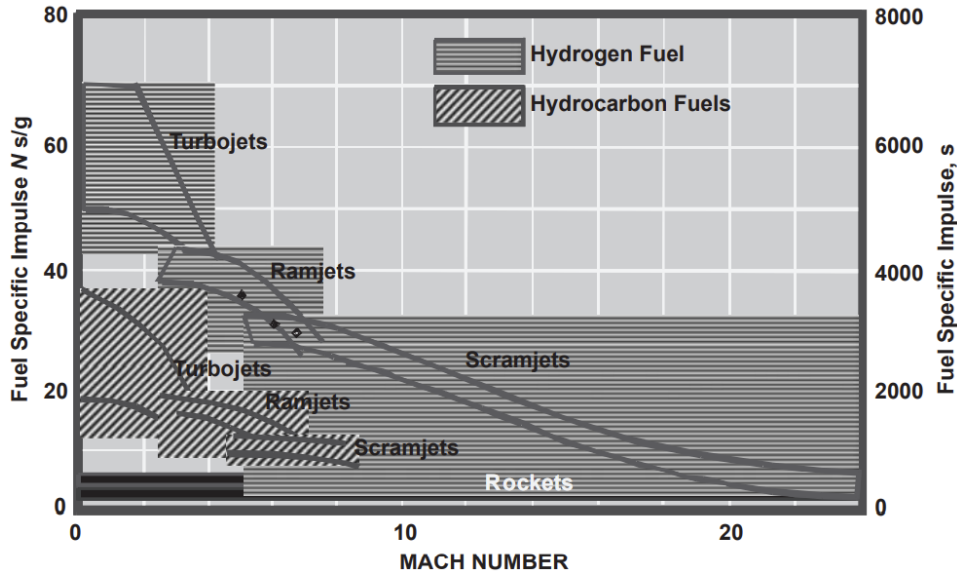
Figure 1.1   Specific impulse of various Air-Breathing engines (plus rocket engine) vs Mach number [20].

A scramjet is a ramjet with supersonic combustion. In other words, the scramjet shares with the ramjet the compression and expansion processes, but they differ in the nature of the combustion process. The combustion in the ramjet engine is subsonic, while it is supersonic in the scramjet engine. This critical detail along with the thrust producing process of a scramjet are discussed in detail in the next section. The figure above showcases the clear advantage of the scramjet cycle in the hypersonic envelop over the most popular airbreathing systems. On one hand, a turbojet is not suitable for hypersonic flight due to its movable parts that could not withstand the pressure and momentum of the airflow. On another hand, the ramjet fixed parts may cope with the supersonic airflow accordingly, however, the cycle will fail due to the subsonic combustion that will produce high temperatures destructive to the structure of the engine and to the thrust produced. As for the rocket, the engine produces considerably the least total specific impulse, especially in the atmospheric level. This fact is a consequence of carrying both the fuel and the oxidizer in the device, which is a characteristic of the rocket engine only. It also explains why rockets are more

efficient in vacuum and are not suitable for sustained flight within denser continua. The limitations of these machines make the scramjet cycle the only airbreathing configuration to achieve continued hypersonic sailing.

1.2   Scramjets now and then

The development of scramjet engines is a result of the efforts made in developing ramjets. Indeed, ramjets were first developed in the 1940s for military purposes in the frame of the Bumblebee program. The first successful ramjet flight-test was the 'Cobra' ramjet. The device reached Mach 2 at an altitude of 20,000 ft. Following this success, many endeavors were done to develop the ramjet further which resulted to promising results. As an illustration, the Talos missile that was introduced into the Fleet in 1955, was powered by a ramjet engine. Almost all military air-launched ramjets were directed by the Naval Air Warfare Center, Weapons Division at China Lake (NAWC/CL). Given the political climate of world during that era, the need to develop reliable guided anti-aircraft missiles grew stronger and the desire to design and investigate new spacecraft propulsion means surfaced. Hence, in the 1950s, the NASA centers started the research on the supersonic combustion which the Navy supported. After the first successful demonstration of a supersonic combustion providing positive net thrust in 1958, the Navy invested in the making of scramjet-powered missile called SCRAM (Supersonic Combustion Ramjet Missile). SCRAM was intended to cruise at Mach 7.5 at an altitude of 100,000 ft or Mach 4 at sea level, for ranges of 350 nmi and 47 nmi respectively. The program lasted until 1977, nevertheless, it shed light on different aspects of the subject. First, it provided an immense database for many configurations of inlets, fuels, injectors, and combustors for a range between Mach 3 to 8. Second, three main limitations to produce a functioning scramjet-powered missiles were found: logistically unsuitable and fuels, the inability to integrate an active Radio Frequency seeker due to lack of space, and the

3

failure to cool the vehicle properly. The following program devised by J. L. Keirsey of APL was successful in the creating of an engine that used conventional hydrocarbon fuels, able to host an active RF seeker, and capable to withstand high temperatures thanks to the passively cooled materials. The engine enabled a flight speed higher than Mach 6. The program continued providing useful insights that pushed the boundaries of the state of art at the time for different sub-disciplines (aerodynamics, systems control, material engineering…), until its termination by the Congress in 1986. [11]

Figure 1.2   Talos Missile (1958) [11].

In 1996, a new program was established to transit hypersonic airbreathing systems from the experimental milieu to the flight environment. The program is a joint effort between NASA

Langley and NASA Dryden research centers and is called 'Hyper-X wind tunnel program'. The Hyper-X program focuses on three main points: risk reduction, flight validation and design predictions, and methods to enhance the scramjets designs. In a report from the American Institute of Aeronautics and Astronautics (1998, p. 2): 'These objectives include experimental, analytical and numerical activities applied to design the research vehicle and scramjet engine; wind tunnel verification of the propulsion-airframe integration, including performance and operability; vehicle aerodynamic and thermal database development; thermal-structural design; boundary layer transition analysis and control; flight control law development; and flight simulation model development.' [2]. One could easily notice the exceptional results of the Hyper-X in the development of the hypersonic experimental aircraft X-43A. The X-43A broke the Guinness record on March 2004 as the fastest aircraft with a speed of Mach 6.8, and it broke its other record on November 2004 with a speed of Mach 9.6 [24]. Although, the flight tests were successful, problems related temperature increase at the forebody of the aircraft unveiled the limitations for possible military and conventional uses of similar aircrafts. Different temperature distributions were recorded of the different tested X-43A aircrafts due to the difference in the alloys and composites employed. [12]

Figure 1.3   NASA X-43 [12]

Other developed countries have shown interest in hypersonic sailing and the development of scramjets. In 2017, a conference co-hosted by the American Institute of Aeronautics and Astronautics (AIAA) and the Chinese Academy of Engineering, and organized by the Xiamen university, took place at the science and arts center of the university. The event was titled 'The 21st International Spaceplane and Hypersonic Systems and Technologies Conference'. Researchers from 18 countries (The US, the EU, China, Japan…) attended the international forum exchange ideas about the state of art of hypersonic sailing technologies. The Chinese researchers particularly have presented interesting updates on scramjets design and tests in China. The first apercu of a Chinese scramjet was in December 2015. The vehicle flew with a speed of Mach 7 at an altitude of 30,000 m. Nowadays, a program directed by Beijin Power Machinery Research Institute is

implemented to create dual-mode ramjet/scramjet vehicles. The rumored vehicle engine consists of two level, in which one has turbines to cater the subsonic flight, and the other contains the ramjet/scramjet engine. The studies are directed to ensure a smooth transition to the Mach 10 register and to lower the thermal damages using innovative and reliable cooling techniques. The first flight-test is expected in 2030. To accompany this project, super hypersonic wind tunnels are being built. As a matter of fact, China possesses the world's largest wind tunnel called JF-12; and the country has plans to build a bigger one whose name is FD-21. While the JF-12 provides a register of Mach 5 to 9, the 170m long FD-21 is predicted to offer speeds of Mach 10 to 15.[7]

1.3 The scramjet thermodynamic cycle

The scramjet engine components are summarized in four main sections: inlet, isolator, combustor, and nozzle. These components exhibit the steps of the Brayton cycle.

Scramjet Thermodynamics Cycle : Brayton Cycle

Ideal process ————
Real process ············

T

Non ideal : entropy increase

Isolator/combustor : Constant pressure heat addition

Qin

4

2

Combustor/ Nozzle : Adiabatic expansion

Inlet/Isolator : Adiabatic compression

Qout

5 ····· 5'

Non ideal : entropy increase

Nozzle/Exit : Constant pressure heat rejection

Non ideal : Incomplete

1

S

P

Isolator/combustor : Constant pressure heat addition

Qin

2 ———— 4

Combustor/ Nozzle : Adiabatic expansion

Inlet/Isolator : Adiabatic compression

Qout

1

5

Nozzle/Exit : Constant pressure heat rejection

V

Figure 1.4   The Brayton thermodynamic cycle

During flight, the incoming flow is slowed down by the inlet section. In ideal settings, the flow undergoes an adiabatic compression as it is captured by the intake. This is achieved thanks to the geometry of the inlet, in lieu of using a mechanical compressor. The goal is to decelerate the incoming flow and prepare it for the combustion process, while maintaining the supersonic state. For this purpose, many inlet designs have been suggested throughout history. One of the most popular types is 2D Planar Designs. This inlet design is the one adopted for the suggested model

8

of this thesis. The 2D-planar inlets use series of arranged oblique shock waves to achieve the desired compression ratio. By incorporating a discrete number (2, 3, or 4) of turns of angles in the profile inlet, the flow is captured and prepped for the following stages of the cycle. The advantage of this type is the ease of design and the facility of introduction of moveable parts in the design. However, to make this design usable for a practical range of flight Mach number, it is necessary to incorporate variable geometry. This is because the number of turnings needed for smaller Mach numbers is greater than higher flight Mach numbers. Other types of inlet designs worthy of mentioning are the outward turning 2D axisymmetric design (e.g., Oswatitsch inlet), are the inward turning 2D axisymmetric design (e.g., Busemann inlet), and the 3D inlet design. [17][22]

After undergoing the compression process, the flow passes through the isolator section. During the combustion process, the pressure rise may cause separation to the flow; and by consequence, hinder the compression process and cause the engine to unstart. To avoid such handicap, a small section characterized by its constant area, is added between the inlet and the burner. This section is called the isolator, whose main goal is to contain the separated flow to avoid engine failure. Typically, a train of oblique shock waves is found in a scramjet's isolator, while a train of normal shockwaves is found in a ramjet isolator.

Following the isolator lies the burner/combustor, where the combustion happens. The combustion chamber may be considered the most important section, since it dictates how the other units behave and is responsible of most of the limiting parameters. The fuel injection and the heat addition cause the pressure to reach its highest. The pressure rise is responsible of length of the shock train contained by the isolator, which is a restrictive factor of the engine. Moreover, thermal choke is most likely to happen in this portion, given the fact that stagnation temperature is increasing, and Mach number is decreasing. Besides, the combustion happens under supersonic

conditions, which induces residence time limitations. Those limitations are co-opted by the three sub-processes found in a typical combustion process: vaporization, mixing, and chemical reaction. Indeed, the vaporization process affect the temperature and the velocity of the fuel and the flow. The mixing should be done on a molecular level and in a rapid manner to ensure that the combustion happens within the combustion chamber. Finally, the chemical reaction should be fast to ensure that the flow is not combustion is not happening throughout nozzle. On the other hand, the combustion should not happen in subsonic conditions. Indeed, starting Mach 6, subsonic combustion may result in very high temperatures that will lead to ionic dissociation instead of a simple chemical oxidization. Not only ion production will result in critical contamination of the engine body and the surrounding air, but also it is an endothermic process that will absorb energy instead of releasing it to produce thrust.

Finally, the flow expands in the nozzle due to area increase and converting thermal energy into kinetic energy to produce thrust.

The analysis presented by this thesis corresponds to engines of the shape showcased by the figure below. An inlet that consists of only external compression, an isolator, a symmetric burner, and a symmetric diverging nozzle. The cross-section area of the engine is rectangular or elliptic.

M3 decrease means :
- n_{th} increase
- Reducing pressure losses
- Reduce n_{KE}
- High pressure rise in the combustor causing boundary seperation in the isolator
- Possibility of thermal choke.

Models :
- Droplet
- Diffusion flame
- Premixed flame

Inlet

Isolator

Combustor

Nozzle

1

2

3

- Slows down the incoming flow using compression ramps that cause oblique shock waves. The process leads to an increase of temperature and pressure.

- Threshold between combustor and upstream shockwaves.

- In case of no disturbance, the flow behaves like Fanno flow.

- If the shocktrain length is greater than the isolator length, the engine fails.

- The supersonic combustion is a must, due to the high temperature rise. If the reaction is subsonic, the high temperature will cause ionic dissociation which is endothermic. Hence, the energy loss will lead to low thrust production and the scramjet structure will be corroded.

Typically, the Damkoler number is 1, which means both chemical and convection effects are equally important. It is desirable to have Da<1 in a scramjet

- The mixing time, vaporization, and reaction rate are the limitting factors.

- The highest pressureoccurs here. If it exceeds Kantrowitz limit, the engine fails.

4

5

- Accelerates flow using expansion fan. The closest to ideal is when the exit static pressure matches ambient pressure.

- In real applications, the flow is both non-isentropic and calorifically imperfect.
- If one of these states could be approximated, the nozzle model can be solid.

- The pressure should not be way smaller than the abient pressure othewise adverse pressure gradient will be created

Total length is of order: 1 m

Total process time is of order: 1 ms

Figure 1.5   Summary of the scramjet engine

Typically, the scramjet engine will have in addition to the shown components an internal inlet and probably and two-stage Nozzle.

1.4   Motivation

In response to the need of faster aerial vehicles, the number of publications in that scope

has skyrocketed in the previous decade, as shown in the presented figures.
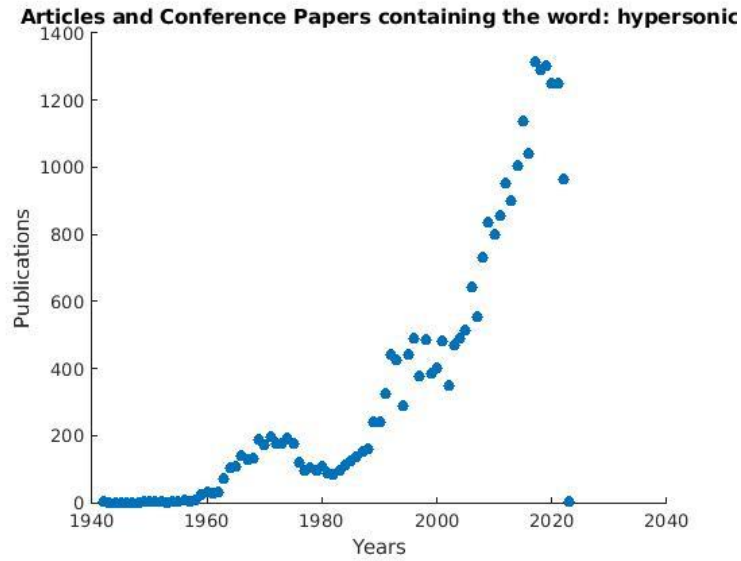
Figure 1.6   Peer-reviewed articles and conference papers containing the word: *hypersonic* (Data obtained from www.scopus.com)
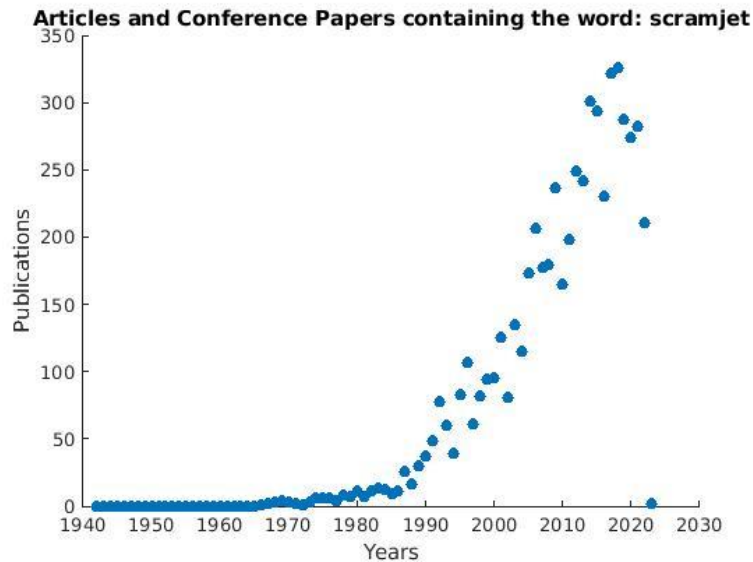
Figure 1.7   Peer-reviewed articles and conference papers containing the word: *scramjet* (Data obtained from www.scopus.com)

To accompany the endeavors done by many research groups to produce more accurate technologies – CFD or experiments, a reduced order model or a 1D model could serve as a

convenient tool to run preliminary tests before investing in a costly study. This explains the need for MSU scramjet 1D model.

There are many models available to perform a "rough" analysis of scramjet engines. Some may be more accurate than the others, however, it is less common to find open-source models that allow to perform parametric studies on the scramjet engine. Indeed, a single parameter changes in the configuration of a scramjet engine could lead to failure or a not sufficient thrust.

In order to produce a model that could be descriptive of the scramjet engine and enable as many configurations as possible, the MSU model is planned to go through three levels. The first level is the subject of this thesis. First, the model needs to assess whether the engine is able to self-start or not. This level is critical and often overlooked, since a configuration may produce a high thrust on theory, but at the same time, it can be also a failing configuration due to a long shock-train. In this level, tools accounting for limiting effects of the self-start of the engine should be implemented. The second level will be achieved by introducing mechanisms enable a decent estimation of the thrust generated by the engine. Finally, the third level is attained by establishing methods to estimate the drag generated within the engine. Indeed, it is worthy to note that this level is immensely important to have in a low-cost tool used for preliminary scanning of the many scramjet configurations. An engine configuration may result in a functioning scramjet engine that will produce a tremendous amount of gross thrust, however, it might result in drag equal in magnitude to the thrust produced.
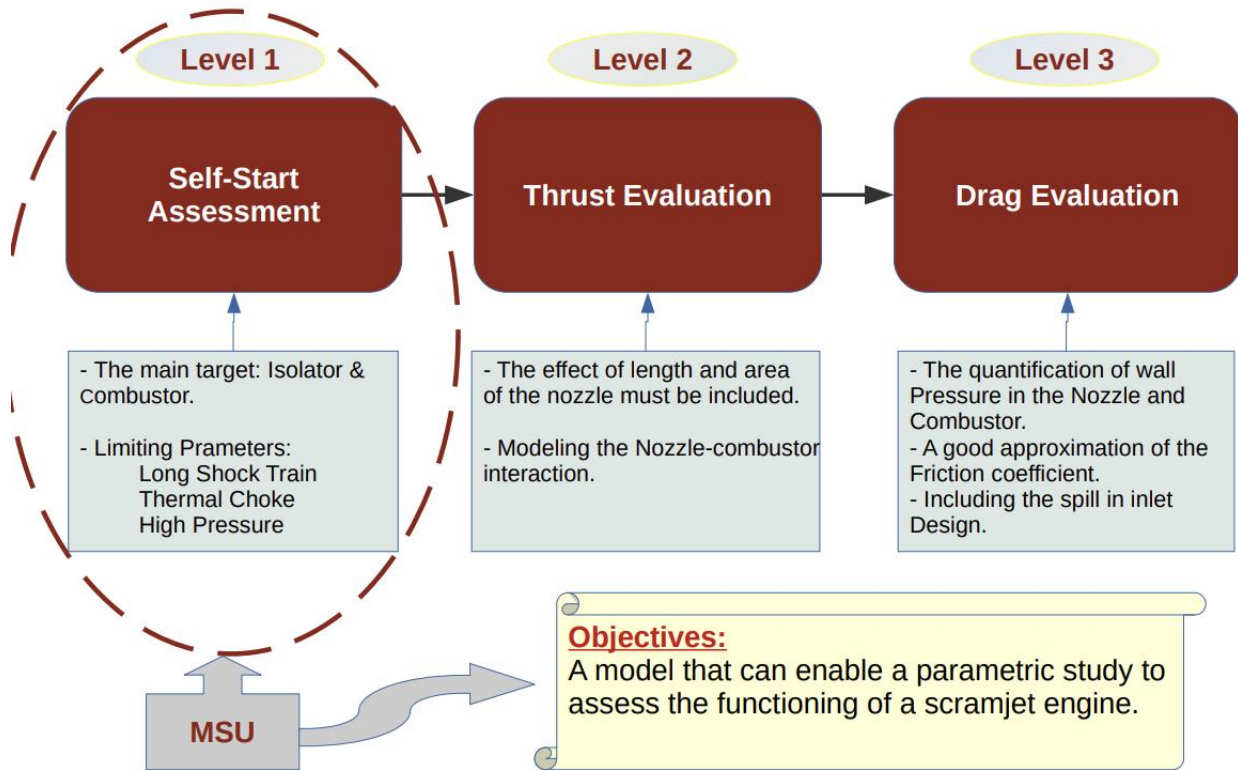
Figure 1.8   Summary of three levels the MSU model is planned to go through.

CHAPTER II

AVAILABLE VALIDATION DATASET

As mentioned before, the goal of this work is to provide a low-cost decisive tool on the functioning of a scramjet engine. Many scramjet 1D models could be found in the literature, however, few could serve as a validation reference. Indeed, there aren't many 1D scramjet models that were verified to experimental data. It is also worthy to mention that one dimensional detailed experimental data is scarce. Fortunately, the 1D models/analysis provided by University of Texas at Arlington in 2015 and 2018 could serve as excellent validation references for both the isolator section and the combustor section. Both models have been verified to experiments for the same sections. The MSU is likewise verified to experimental data used in both papers: Fisher experiment for the isolator and Boyce experiment for the combustor.

2.1   University of Texas at Arlington 2015

The model envelops both the scramjet and the ramjet modes. In addition, it provides an extensive analysis of the critical components of the scramjet. The isolator model of this package utilizes the thermally perfect gas assumption instead of the calorically perfect gas assumption. The TPG assumption is more useful at high temperatures, given the fact it represents the vibrational energy the gas gains at this register. Since the temperature within the isolator is high due to the compression undergone in the inlet, a TPG assumption is more suitable for this application. The TPG assumption has been kept for both the attached flow solver (shock free

region) and the shock train region; the later has been solved through an internal shock reflections solver in two confined wedges. The said model had shown accuracy compared to experiments.

For the combustor, the university of Texas at Arlington 2015 model follows a detailed strategy to represent the flow dynamics sophistically. First, the combustor is divided into two regions: injector and combustion chamber. For the fuel injection sub-model, many critical properties have been evaluated. The most important parameter is the area change due to the geometry and type of injector, and the wake of the jet injection. As explained in Chapter 5, the confined flow cross section area directly influences the flow properties, namely the pressure. Another important parameter is the axial component of the velocity of injection jet, which affects the momentum of the flow and its internal energy. The burner (combustion chamber) model uses the modified momentum equations, and the revised energy equations with volumetric heat addition and wall heat flux. A more elaborate chemical reaction scheme was used to calculate the varying species mass fractions. Likewise, the model had proven good reliability with respect to experimental data.[10]

2.2   University of Texas at Arlington 2018

Long Vu (2018) had presented a quasi 1D solver for scramjet combustor based on numerical propulsion system simulation, often abbreviated 'NPSS'. The NPSS is a collaborative engine simulation software developed by NASA Glenn Research Center under NASA's High Performance Computing and Communication Program. It is basically a 'virtual wind tunnel' integrating multiple disciplines (Fluid mechanics, heat transfer, controls…) to visualize the behavior and interaction of multiple components within the engine. The purpose behind developing the NPSS is to provide a tool that will permit a rapid, affordable, and stable object-oriented computation simulation. A simulation as such will facilitate the production and

16

manufacturing of engines in the aeronautical industry by decreasing the time and resources spent on experiments and certification requirements [14].

University of Texas at Arlington 2018 model uses the NPSS to simulate the flow dynamics at the combustor and the isolator. Similar equations used in the 2015 model has been used in the 2018 model in the combustor section. As for the isolator section, the equations used in the combustor were kept while the sub-routines related to heat addition were turned off. Changes related to core flow area change were brought to accommodate the flow separation case. The model was as well validated with Boyce experiment for the burner section, and Fisher experiment for the isolator section.[28]

2.3   Fisher Experiment

The experiment was part of Germany's research training group (GRK 1095) "Aero-Thermodynamic Design of a Scramjet Propulsion System for Future Space Transportation Systems". The purpose of the research is to investigate the inlet isolator flow path for different yaw angles and to characterize the isolator flow field. The isolator discussed is a duct with a rectangular cross-section area. Many configurations were tested, some with heated walls and others with unheated walls. The purpose behind such a choice is to examine the effect of total temperature and the wall temperature on the length of the shock train. The experiment was divided mainly in two free stream conditions. While according to Fisher, Condition II is closer to flight conditions with respect to total enthalpy, the MSU model will be verified to Condition I. Not only Condition I represents flow cases with little heat transfer, but also both models suggested by university of Texas at Arlington were verified to the cases falling in Condition I category. Condition I was chosen, given the fact that, the MSU model does not cover the heat transfer effects at the isolator and the model is verified with the aforesaid models. C. M. Fisher

17

used the hypersonic shock tunnel TH2 to create a free stream of helium and the isolator is mounted parallel to a plate. The inflow is then decelerated upon reaching the plate, as the later induces a single shockwave to the incoming flow. The plate-isolator unit are tilted to fit different angles of attack in order to generate different isolator entry Mach numbers M_2. To generate a pressure jump at the exit of the isolator, a movable wedge was deployed. The value of the induced pressure rise is determined experimentally [8].

2.4 Boyce Experiment

A ground test had been performed by R. R. Royce to compare between the dynamics of the supersonic combustion in a vitiation-heated blowdown tunnel and a free-piston shock tunnel. The facilities represent an example of a long-duration facility and a short-duration facility, respectively. Cases for different combustion equivalence ratios were executed, and an agreement between the results of the two installations has been achieved. The experiment was accomplished at the university of Queensland. The experiment describes an incoming flow goes through a constant area rectangular duct (isolator), then, through a diverging duct where a strut injector was placed; the fuel used is Hydrogen fuel. The MSU model will be verified to the findings of the shock tunnel equipment, given that the previous models were verified to this case. [5] [10]

CHAPTER III

INLET MODEL

To model the inlet, an approach based on isentropic flow characteristics has been developed. The figure below represents a schematic of a 2D planar inlet with a single turn. The reason behind adopting such method is to produce a model that quantify the effect of the ramp angle and flight conditions on the scramjet functioning.
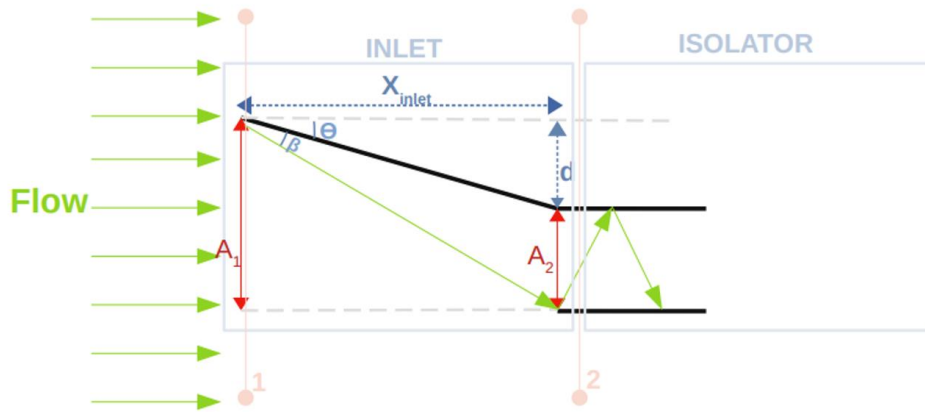
Figure 3.1   Schematic of the Scramjet inlet.

The incoming flow is met with the inlet ramp of angle θ. Due to the supersonic nature of the flow, this situation will result to the production of a shockwave of angle β as shown in the schematic. By solving the equation below, the shock angle β could be found [16].

$$\tan \theta = 2 \cot \beta \left[\frac{M_1^2 \sin^2 \beta - 1}{2 + (\gamma + \cos 2\beta) M_1^2} \right] \tag{3.1}$$

The user enters the angle θ and the flight Mach number M_1. The model then calculates

the angle β using the Newton-Raphson method.

$$f(\beta) = 2\cot\beta \left[\frac{M_1^2 \sin^2\beta - 1}{2 + (\gamma + \cos 2\beta)M_1^2}\right] - \tan\theta \qquad (3.2)$$

$$\beta_{i+1} = \beta_i - \frac{f(\beta)}{f'(\beta)}$$

The code iterates until it reaches an error of 10^{-5}. An approximation on β's value for high speeds

have been provided. Indeed, it was observed that β becomes independent of Mach number as the

flight speed is getting higher. Overall, in hypersonic conditions β was found to approach $\beta \approx$

$\frac{(\gamma+1)}{2}\theta$ [20]. To avoid divergence of the solution, this approximation is implemented as the first

guess for the code. Following this strategy, many combinations of M_1 and θ have tested and no

divergence have occurred.
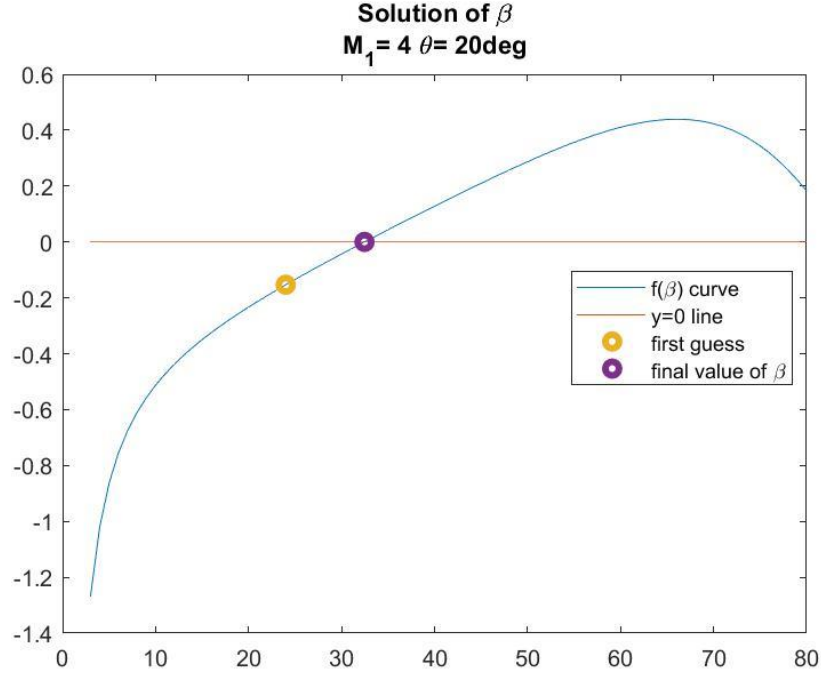
Figure 3.2   Plot of the function $f(\beta)$, the first guess and the estimated solution.

       After the shockwave angle is obtained, the flow properties following the compression are calculated following the equations below. The stagnation relations were used to determine the Mach number after the shockwave.

$$\frac{P_2}{P_1} = 1 + \gamma\, M_1^2 \sin^2 \beta \left(1 - \frac{\rho_1}{\rho_2}\right) \tag{3.3}$$

$$\frac{T_2}{T_1} = 1 + \frac{\gamma - 1}{2}\, M_1^2 \sin^2 \beta \left(1 - \left(\frac{\rho_1}{\rho_2}\right)^2\right) \tag{3.4}$$

$$\frac{\rho_2}{\rho_1} = \frac{(\gamma + 1)\, M_1^2 \sin^2 \beta}{2 + (\gamma - 1) M_1^2 \sin^2 \beta} \tag{3.5}$$

$$\frac{\frac{T_{st}}{T_2}}{\frac{T_{st}}{T_1}} = \frac{T_1}{T_2} = \frac{1 + \frac{\gamma - 1}{2} M_2^2}{1 + \frac{\gamma - 1}{2} M_1^2}$$

$$M_2 = \left(\frac{2}{\gamma - 1}\left[\frac{T_1}{T_2}\left(1 + \frac{\gamma - 1}{2} M_1^2\right) - 1\right]\right)^{\frac{1}{2}} \tag{3.6}$$

The flight flow properties are obtained by interpolating the U.S. standard air atmosphere table. Once the user enters the altitude of the flight, the code generates the flow initial properties from the USSA table.

Geo potential Altitude above Sea Level - h - (m)	Temperature - t - (°C)	Acceleration of Gravity - g - (m/s²)	Absolute Pressure - p - (10⁴ N/m²)	Density - ρ - (kg/m³)	Dynamic Viscosity - μ - (10⁻⁵ N s/m²)
-1000	21.50	9.810	11.39	1.347	1.821
0	15.00	9.807	10.13	1.225	1.789
1000	8.50	9.804	8.988	1.112	1.758
2000	2.00	9.801	7.950	1.007	1.726
3000	-4.49	9.797	7.012	0.9093	1.694
4000	-10.98	9.794	6.166	0.8194	1.661
5000	-17.47	9.791	5.405	0.7364	1.628
6000	-23.96	9.788	4.722	0.6601	1.595
7000	-30.45	9.785	4.111	0.5900	1.561
8000	-36.94	9.782	3.565	0.5258	1.527
9000	-43.42	9.779	3.080	0.4671	1.493
10000	-49.90	9.776	2.650	0.4135	1.458
15000	-56.50	9.761	1.211	0.1948	1.422
20000	-56.50	9.745	0.5529	0.08891	1.422
25000	-51.60	9.730	0.2549	0.04008	1.448
30000	-46.64	9.715	0.1197	0.01841	1.475
40000	-22.80	9.684	0.0287	0.003996	1.601
50000	-2.5	9.654	0.007978	0.001027	1.704
60000	-26.13	9.624	0.002196	0.0003097	1.584
70000	-53.57	9.594	0.00052	0.00008283	1.438
80000	-74.51	9.564	0.00011	0.00001846	1.321

Figure 3.3   The U.S. Standard Air Atmosphere Table in S.I. units [27]

From the steady-state lens, there are some parameters affecting the inlet self-starting conditions. The internal contraction ratio, the pressure recovery, and the local Mach number are the main parameters to be studied. Studies have proven that a certain criterion is used to estimate

the internal contraction ratio that will allow the inlet to self-start. This criterion is known as the Kantrowitz limit:

$$\left(\frac{A_1}{A_2^*}\right)_{KANTROWITZ}$$

$$= \frac{1}{M_2}\left[\frac{(\gamma+1)M_1^2}{(\gamma-1)M_1^2+2}\right]^{\frac{\gamma}{\gamma-1}}\left[\frac{(\gamma+1)}{2\gamma M_1^2-(\gamma-1)}\right]^{\frac{1}{\gamma-1}}\left[\frac{1+\gamma-\frac{1}{2}M_1^2}{\gamma+1/2}\right]^{\frac{\gamma+1}{2(\gamma-1)}} \tag{3.7}$$

The formula above is found by assuming a normal shock wave in the inlet's throat. In other words, the flow was compressed to the sonic state after shockwave. For isentropic process, the formula is further simplified to:

$$CR = \left(\frac{A_1}{A_2^*}\right)_{isentropic} = \frac{1}{M_1}\left[\frac{2}{\gamma+1}\left(1+\frac{\gamma-1}{2}M_1^2\right)\right]^{\frac{\gamma+1}{2(\gamma-1)}} \tag{3.8}$$

The capture area is known following the Eq 3.8, the properties after the shockwave, and the initial area of the intake.

$$\frac{A_2}{A_1} = \frac{A_2}{A^*}\frac{A^*}{A_1} = \frac{A_2}{A^*}\frac{1}{CR}$$

$$A_2 = A_1\frac{1}{CR}\frac{1}{M_2}\frac{\rho^*}{\rho_2}\sqrt{\frac{T^*}{T_2}} \tag{3.9}$$

The captured mass flow rate is then found to be:

$$\dot{m}_{air} = \rho_2\,A_2\,M_2\,\sqrt{\gamma R T_2} \tag{3.10}$$

It is important to note that the maximum pressure that a functioning scramjet would reach is P', which is the pressure after the assumed normal shockwave. If the pressure within the scramjet reaches a value higher than P', the engine would fail. Hence, knowing the upper-limit of the pressure is a necessity to design and operate the engine.

$$P' = \frac{P_t}{\left[\frac{\gamma + 1}{2}\right]^{\frac{\gamma}{\gamma - 1}}}$$

(3.11)

For the current design, an elliptic/circular cross-section profile has been assumed. Starting from the data acquired about the inlet's geometry, the length of the section could be computed as follows.
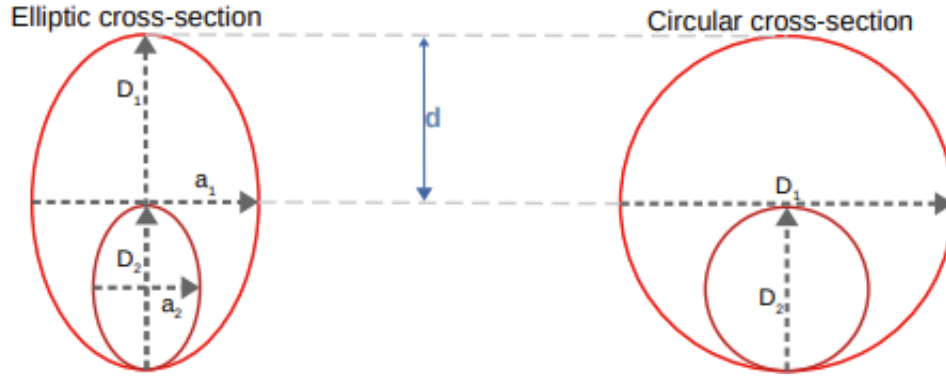
Figure 3.4   Inlet Cross-section area.

After an examination of the geometry of inlet, the formula below has been found.

$$d + D_2 = D_1$$

$$D_2 = D_1 - d$$

$$A_2 = \frac{\pi}{4} D_2^2 = \frac{\pi}{4} (D_1 - d)^2$$

$$D_1^2 - 2D_1 d + d^2 = \frac{4}{\pi} A_2$$

For an ellipse:

$$d^2 - 2D_1 d + \left(D_1^2 - \frac{4}{\pi r_D} A_2\right) = 0$$

(3.12)

For a rectangle:

$$d^2 - 2D_1 d + \left(D_1^2 - \frac{A_2}{r_D}\right) = 0$$

(3.13)

24

Where, $r_D = \frac{a_1}{D_1} = \frac{a_2}{D_2}$ (The same ratio is assumed for both ellipses or rectangles) and knowing that:

$$d = X_{inlet} \tan \theta \qquad (3.14)$$

The polynomial has two roots, one is less than D_1 while the other is greater than D_1 . The

solution to the problem at hand is the root satisfying $d < D_1$.

To summarize, the user enters the altitude, the Mach number, and the ramp angle. The model

calculates the flow properties by interpolating the USSAA table. Then, using the flight Mach

number and the ramp angle, the shockwave angle is approximated using Newton-Raphson method.

Following this step, the model proceeds to calculate the flow properties post the shockwave. Those

results are used to estimate the useful geometry of the inlet for these specific conditions. The

parameters calculated are the capturing area and the inlet length. Finally, the captured mass flow

rate is estimated along with the allowable pressure upper limit of the cycle. An example of the

code results is presented.

Table 3.2   An example of an implementation of inlet model: inputs

Inputs	
Flight Mach number M_1	4
Altitude h in m	0
Inlet's initial parameter D_1 in m	1
Aspect ratio r_D	1
Ramp angle θ in degrees	20

The model displays the flow characteristics at the free stream conditions and at the exit of

the inlet in the following manner:

Table 3.3   An example of an implementation of inlet model: Results

	Free Stream	Inlet Exit
Mach Number	4	2.57
Pressure in Pa	101300	527915
Temperature in K	288.15	521.74
Density kg/m^3	1.225	3.526

Further information about this configuration is displayed. Indeed, the inlet choke area is

$7.162 \ 10^{-3} \ m^2$ and the length of the section is 2.485 m. The mass flow rate captured is 29.7

kg/s. The upper limit of the pressure for the tested flight Mach number is $8.12 \ 10^6 \ Pa$. The jump

of the characteristics of the flow is showcased in the plots below.
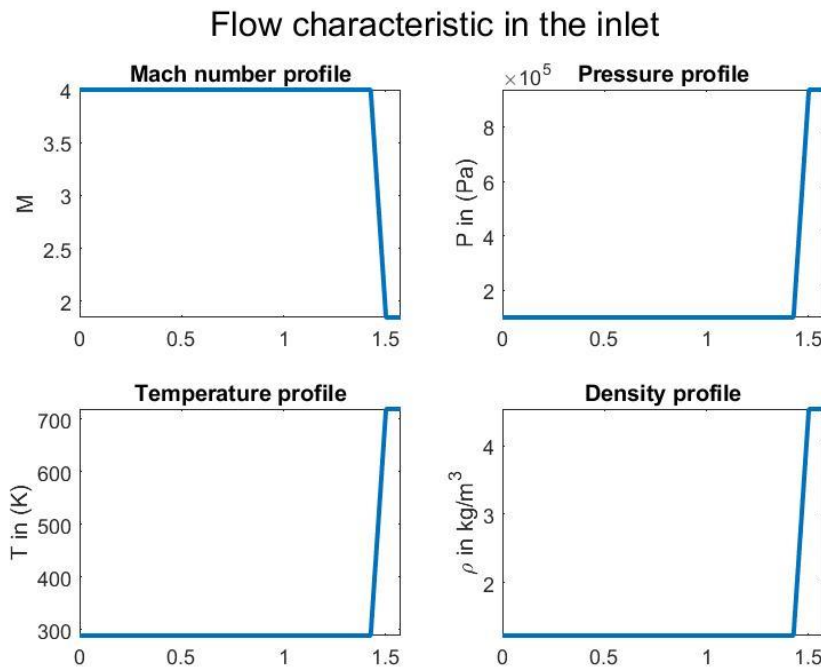
Figure 3.5   Characteristics of the flow in the inlet.

The location of the jump has been calculated based on the centerline of the captured flow.

Using Thales proportionality theorem, the analysis has given:
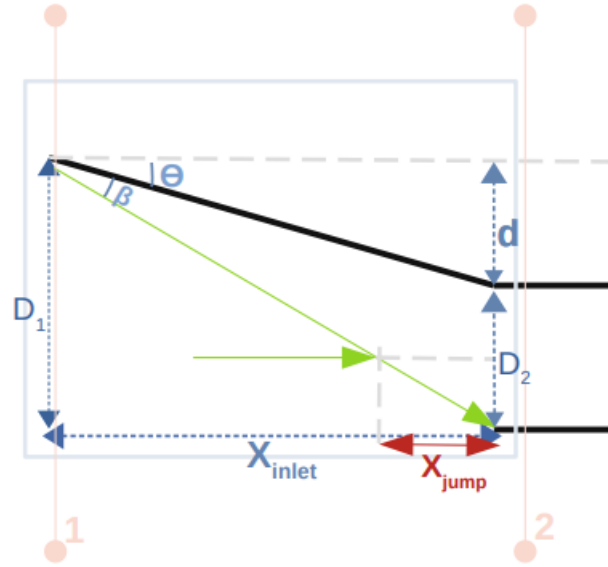
Figure 3.6   Second schematic of the Scramjet inlet.

$$\frac{D_2}{2}\Big/D_1 = X_{jump}\Big/X_{inlet} \tag{3.15}$$

$$X_{jump} = X_{inlet}\,\frac{D_2}{2D_1} = X_{inlet}\,\frac{D_1 - d}{2D_1} \tag{3.16}$$

CHAPTER IV

ISOLATOR MODEL

The flow within the isolator could be divided into two portions: the attached flow and the separated flow. The attached flow with the isolator is treated and modeled according to Fanno flow characteristics. Indeed, the flow is assumed to be adiabatic and passing through a constant area duct with friction effects. The combustor's pressure rise induces separation and an oblique shock train as shown in the figure below. The detached flow is modeled following separated flow equations found in [18] and [21].
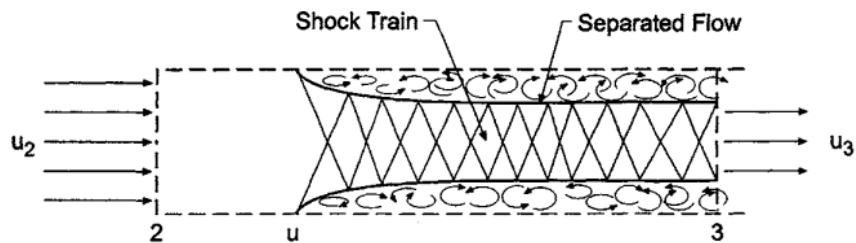
Figure 4.1   Isolator with separation [17]

To validate the isolator model, the test configurations described in [10] and [8] have been used as verification references. The conditions of four cases of an isolator with flow separation were entered in the model and acceptable results were obtained. The location of the separation point was calculated following the strategy explained in Chapter 6.

4.2   Attached Flow

Assuming the free body diagram shown below:
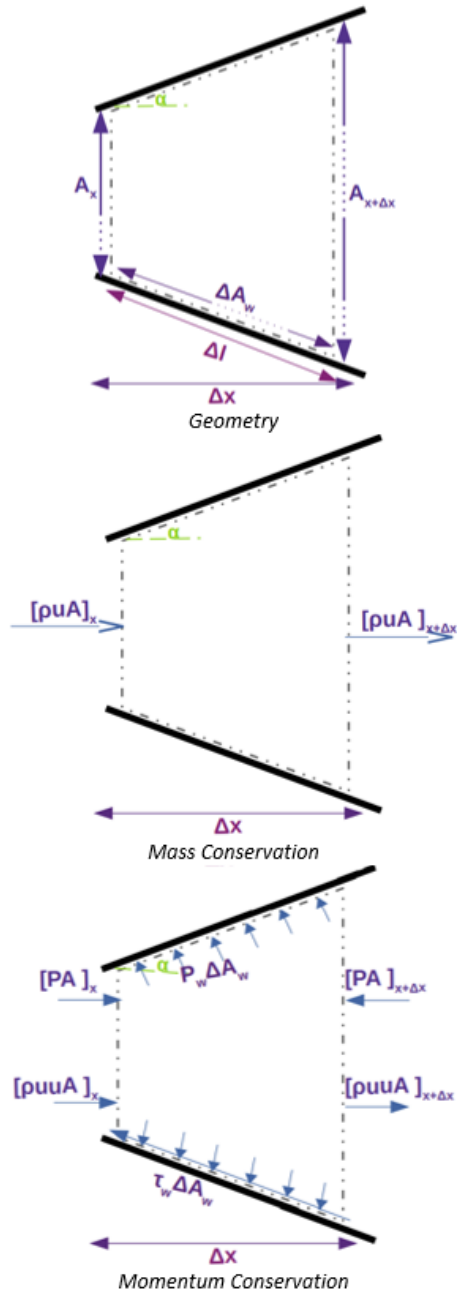
Figure 4.2   FBD of inviscid flow in a duct

The equations are found for mass conservation, momentum conservation, and energy conservation are:

Continuity:

$$[\dot{m}]_x = [\dot{m}]_{x+\Delta x} \tag{4.1}$$

We get as $\Delta x \sim 0$,

$$d\dot{m} = 0 \tag{4.2}$$

$$d(\rho u A) = 0 \tag{4.3}$$

Finally,

$$\frac{du}{u} + \frac{d\rho}{\rho} + \frac{dA}{A} = 0 \tag{4.4}$$

Momentum Conservation:

$$[\dot{m}u]_{x+\Delta x} - [\dot{m}u]_x = [PA]_x - [PA]_{x+\Delta x} + P_w \sin(\alpha) \, dA_w - \tau_w \cos(\alpha) \, dA_w \tag{4.5}$$

$$[\rho u^2 A]_{x+\Delta x} - [\rho u^2 A]_x = [PA]_x - [PA]_{x+\Delta x} + P_w \sin(\alpha) \, dA_w - \tau_w \cos(\alpha) \, dA_w \tag{4.6}$$

Dividing by Δx, and taking the limit of $\Delta x \sim 0$ and taking into consideration mass conservation:

$$\rho u A \frac{du}{dx} = -A\frac{dP}{dx} - P\frac{dA}{dx} + P_w \sin(\alpha)\frac{dA_w}{dx} - \tau_w \cos(\alpha)\frac{dA_w}{dx} \tag{4.7}$$

Energy Conservation:

$$[\dot{m}h]_x + \left[\frac{1}{2}\dot{m}u^2\right]_x = [\dot{m}h]_{x+\Delta x} + \left[\frac{1}{2}\dot{m}u^2\right]_{x+\Delta x} + q_w''' dA_w \tag{4.8}$$

Dividing by Δx, and taking the limit of $\Delta x \sim 0$:

30

$$\rho u A \frac{d}{dx}\left(\int c_p \ dT + \frac{1}{2}u^2\right) = -q_w''' dA_w \qquad (4.9)$$

Where q_w''' is the volumetric heat rate transferred to the walls of the engine.

Adopting the following assumptions:

- 1D, Steady state

- Constant area

- Negligible radiation

- No heat exchange with the walls.

- Constant specific heats

The equations become:

$$\frac{du}{u} + \frac{d\rho}{\rho} = 0 \qquad (4.10)$$

$$\rho u A \frac{du}{dx} = -A \frac{dP}{dx} - \tau_w \frac{dA_w}{dx} \qquad (4.11)$$

$$c_p \frac{dT}{dx} + \frac{1}{2}\frac{du^2}{dx} = 0 \qquad (4.12)$$

With $\tau_w = \rho \ C_f \frac{u^2}{2}$, $dA_w = p_e \ dx$. p_e is the perimeter of the isolator cross-section.

The hydraulic diameter is given by: $D_H = \frac{4A}{p_e}$. Hence, Eq.4.11 becomes:

$$\rho u \frac{du}{dx} = -\frac{dP}{dx} - 4\rho \ C_f \frac{u^2}{2 \ D_H} \qquad (4.13)$$

Using the definitions of ideal gas and speed of sound: $P = \rho \ R \ T$, $a^2 = \frac{u^2}{M^2} = \frac{\gamma P}{\rho}$, and

combining the equations into the flow governing equations, the following expressions are found:

$$\frac{d\rho}{\rho} + \frac{du^2}{u^2} = \frac{dP}{P} + \frac{dM^2}{M^2} \qquad (4.14)$$

$$\frac{dM^2}{M^2} = 2\frac{du}{u}\left(1 + \frac{\gamma - 1}{2}M^2\right) \tag{4.15}$$

$$\frac{dM^2}{M^2} = \frac{1 + \frac{\gamma - 1}{2}M^2}{1 - M^2}\frac{4\,\gamma\,C_f\,M^2}{D_H}dx \tag{4.16}$$

$$\frac{dP}{dx} = P\frac{2\gamma C_f M^2}{D_H}\frac{1 - 2 - (\gamma - 1)M^2}{1 - M^2} \tag{4.17}$$

The Eq.4.16 and Eq.4.17 were solved using the 4th order Runge-Kutta method.

4.3   Detached Flow

When the flow is separated, the detached flow has a supersonic core region and subsonic regions by the walls. Smart (2008) had provided the governing equations of a separated flow. The mass, momentum, and energy conservation equations were written to account for the area of the core flow A_c. The free body diagram for a separated flow was provided by Smart (2008):
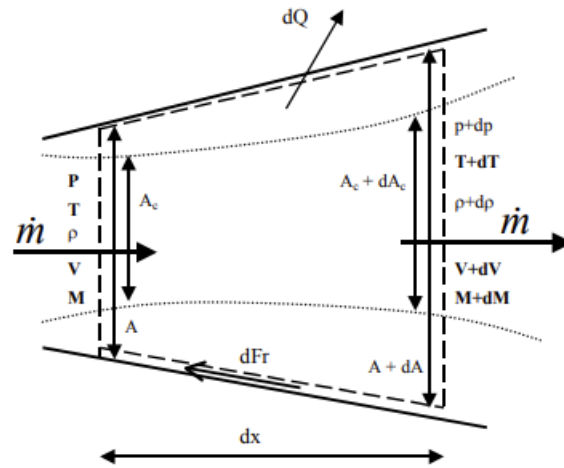
Figure 4.3   Separated Flow FBD [21][22].

Mass conservation:

$$\frac{d\rho}{\rho} + \frac{du}{u} + \frac{dA_c}{A_c} = 0 \tag{4.18}$$

Momentum conservation:

$$\frac{dP}{P} + \frac{\gamma\,M^2}{2}\,\frac{4\,C_f\,dx}{D_H} + \frac{\gamma\,M^2}{2}\,\frac{A_c}{A}\,\frac{du^2}{u^2} = 0 \tag{4.19}$$

The equations given by Smart (2008) are:

$$\frac{dM^2}{M^2} = -\left(1 + \frac{\gamma - 1}{2}M^2\right)\left[\frac{dP/P}{\frac{\gamma\,M^2}{2}\frac{A_c}{A}} + \frac{4\,C_f\frac{dx}{D_H}}{\frac{A_c}{A}} + \frac{dT_t}{T_t}\right] \tag{4.20}$$

$$\frac{d\left(\frac{A_C}{A}\right)}{A_c/A} = \left[\frac{1 - M^2\left(1 - \gamma\left(1 - \frac{A_c}{A}\right)\right)}{\gamma\,M^2\frac{A_c}{A}}\right]\frac{dP}{P} + \left[\frac{1 + (\gamma - 1)M^2}{2\frac{A_c}{A}}\right]4\,C_f\frac{dx}{D_H}$$

$$+ \left(1 + \frac{\gamma - 1}{2}M^2\right)\frac{dT_t}{T_t} \tag{4.21}$$

The variable A_c is dependent on the characteristics of the core flow, hence, an additional

equation to bring closure to the system is essential. Fortunately, an empirical formula for the

pressure gradient was provided by Ortwerth (2001) [18]. Based on a large database of

experiments of various configuration of ducts geometries, Mach numbers, and Reynolds

numbers, the pressure gradient formula suggested by the same source is:

$$\frac{d(P/P_i)}{P/P_i} = 4K(P/P_i)M^2 \tag{4.22}$$

Where $4K = 44.5\,C_{fs}$. C_{fs} is the friction coefficient at the separation point. A useful

approximation for pressure gradient is:

$$\frac{dP}{dx} \sim \frac{89\,C_f}{D_H}\,\frac{\rho\,U^2}{2} \tag{4.23}$$

33

The length of the shock train could also be approximated by a correlation presented by Ortwerth (2001) for entrance Mach numbers ranging from 1.5 to 5 [26]. The formula could be used for ducts of rectangular or circular cross-sections with an accuracy of 20%.

$$\frac{X_{shock}}{D_H} = \frac{1}{4K}\frac{g_2^2}{\gamma f_2}\left[\frac{P_r - 1}{(f_2 - P_r)(f_2 - 1)} + \frac{1}{f_2}\ln\left(P_r\frac{f_2 - 1}{f_2 - P_r}\right)\right] + \frac{(\gamma - 1)}{2\gamma}\ln(P_r) \tag{4.24}$$

Where $4K = 44.5\ C_f$, $g_2 = \dot{m}\sqrt{(\gamma - 1)h_t}/P_2 A_2$, $f_2 = F/P_2 A_2$. F is the free stream function at the entry of the isolator such that, $F = P_2 A_2 + \dot{m}u_2$.

Condensing all the discussed aspects of this section, the governing equations of the separated flow are solved to find the flow characteristics within the separated region. Using a nonstiff ordinary differential equation solver ODE45 [23], the following 3 equations were solved simultaneously:

$$\frac{dP}{dx} = P\frac{89\gamma C_f M^2}{2D_H} \tag{4.25}$$

$$\frac{dM^2}{M^2} = -\left(1 + \frac{\gamma - 1}{2}M^2\right)\left[\frac{\frac{dP}{P}}{\frac{\gamma M^2}{2}\frac{A_c}{A}} + \frac{4\,C_f\frac{dx}{D_H}}{\frac{A_c}{A}}\right] \tag{4.26}$$

$$\frac{d\left(\frac{A_C}{A}\right)}{A_c/A} = \left[\frac{1 - M^2\left(1 - \gamma\left(1 - \frac{A_C}{A}\right)\right)}{\gamma M^2\frac{A_c}{A}}\right]\frac{dP}{P} + \left[\frac{1 + (\gamma - 1)M^2}{2\frac{A_c}{A}}\right]4\,C_f\frac{dx}{D_H} \tag{4.27}$$

4.4   Isolator Validation

To verify the isolator model, Fisher experiment and the university of Texas at Arlington models as verification references. The verification cases represent an isolator with a flow

separation. Borrowing the schematic from [10], the experimental set up is simplified in the figure below:
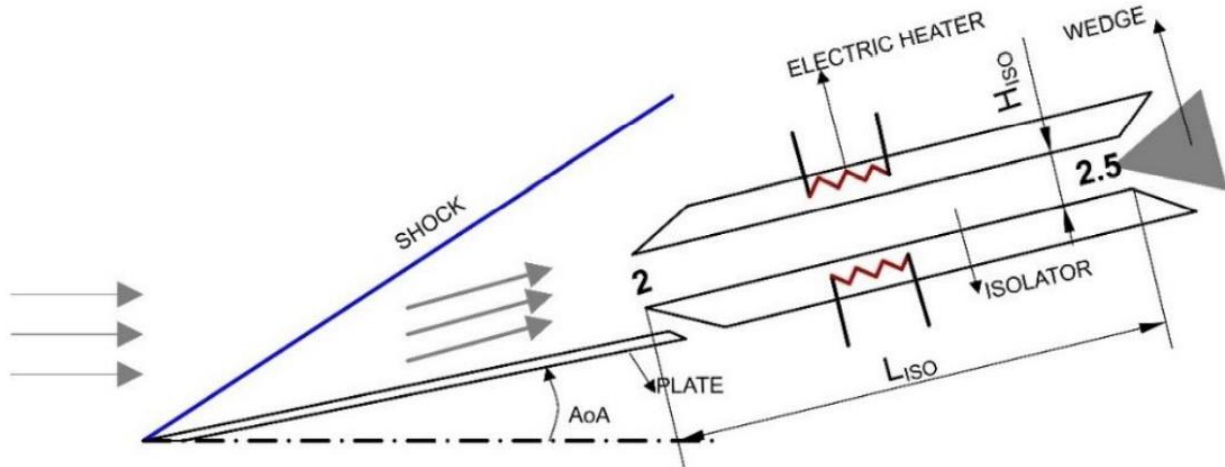
Figure 4.4   Isolator Experimental Setup Schematic [10]

As explained in section 2.3., the incoming flow is compressed due to the tilted plate. The decelerated flow enters the isolator and responds to the back pressure induced by the wedge at the exit of the isolator. The measurements have been done only on the heated portion whose length is 0.18m. The isolator's height and width are 0.018m and 0.1m, respectively. To approximate the input values to the references discussed, NASA polynomials for helium have been used to approximate the specific heat c_p, the gas constant R using $R = \frac{8.314}{MW_{He}}$, and finally and the specific heat ratio γ using $\gamma = \frac{c_p}{c_p - R}$. Since the experiments and the models include the influence of wall temperature on the flow, similar formulas have been used to approximate the friction coefficient. The set of formulas is the following [10], [28], and [8]:

$$Pr = 0.715$$

$$T^* = 0.5T + 0.5T_w + \frac{0.16 \, Pr^{1/3} \, (\gamma - 1)TM^2}{2} \tag{4.28}$$

$$\rho^* = \rho \frac{T}{T^*} \tag{4.29}$$

$$\mu^* = \mu_{ref} \left(\frac{T^*}{T_{ref}}\right)^{\frac{3}{2}} \frac{T_{ref} + 111K}{T^* + 111K} = 1.87 \, 10^{-5} \left(\frac{T^*}{273.15K}\right)^{\frac{3}{2}} \frac{273.15K + 111K}{T^* + 111K} \tag{4.30}$$

$$Re_x^* = \frac{\rho^* \, u \, L}{\mu^*} \tag{4.31}$$

$$C_f^* = \frac{0.02296}{(Re^*)^{0.139}} \tag{4.32}$$

The friction coefficient used in calculations is the average of the computed friction coefficient. The algorithm used is similar to algorithm discussed chapter 6.2. the combustor-isolator interaction model. The pressure profile is presented in terms of the pressure coefficient, such that:

$$C_p = \frac{P - P_0}{\frac{1}{2}P_0\gamma_0 M_0^2}$$

The values tabulated in [Gopal] are adopted for comparison purposes. Hence, $P_0 = 460 \, Pa$, $M_0 = 7.5$, and $\gamma_0 = 1.667$. The test values of the four cases are summarized in the table below according to [10]:

Table 4.2   Isolator Verification Cases Setup [10]

CASE	Isolator Entry Mach Number	Isolator Entry Pressure in Pa	Isolator Entry Temperature in K	Isolator Exit Pressure in Pa	Isolator Wall Temperature in K
1	3.5	12,440	333	40921	1000
2	3.5	12,440	333	30643	1000
3	3.5	12,440	333	27894	1000
4	3	16,320	411	57393	800

The results of the model are presented in the following tables:

Table 4.3   Pressure Profile of the Verification Cases of the Isolator Section.

CASE	Pressure Profile
1	
2	

Table 4.3 (continued)

3	
4	
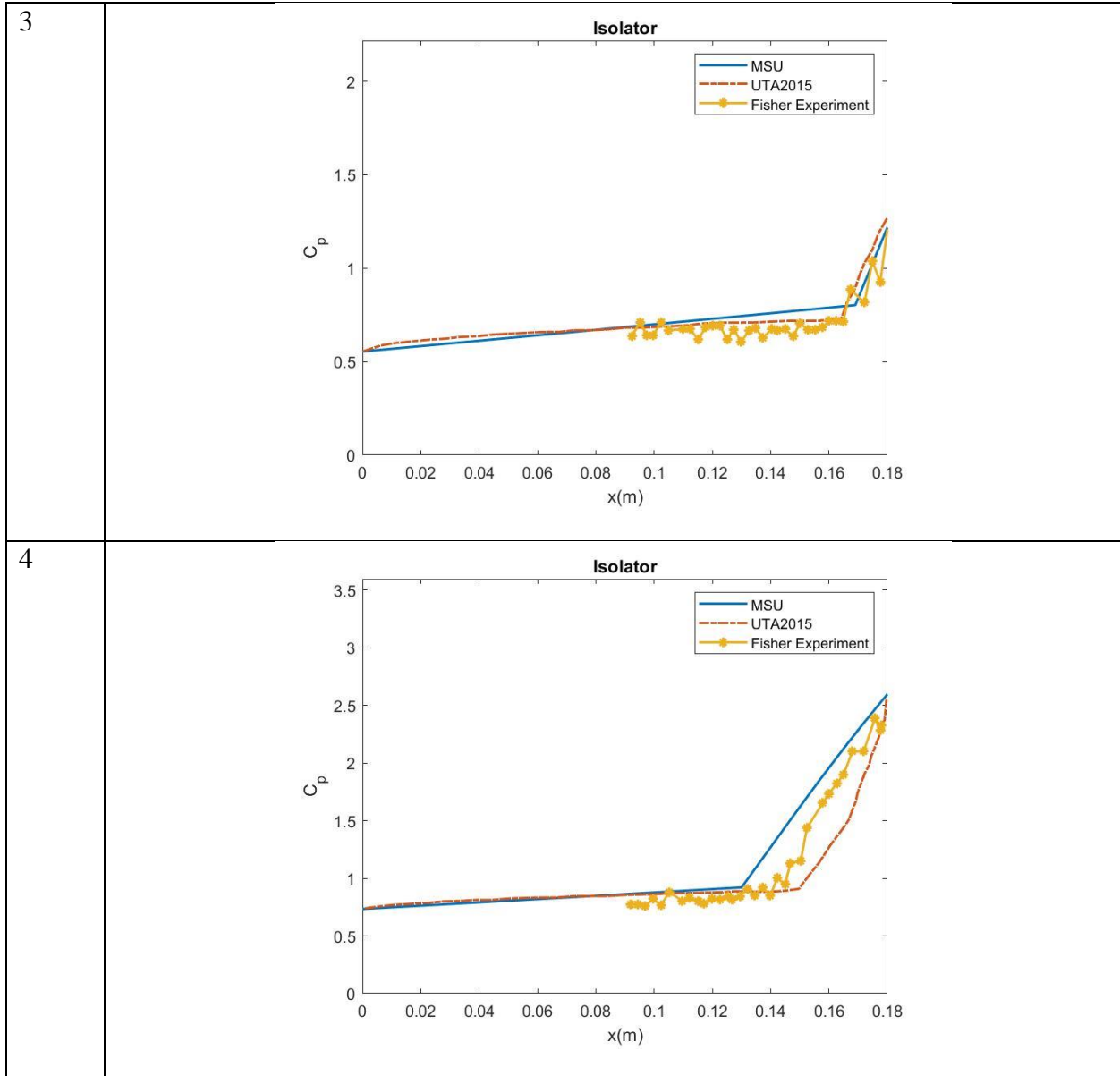
Table 4.4   Isolator Exit Mach Number Validation

Isolator Exit Mach Number			
Experiment	UTA 2015	UTA 2018	MSU
2.1	1.88	2.395	1.8698
2.3	2.23	2.595	2.2152
2.4	2.4	2.677	2.3501
1.7	2.48	-	1.4822

The model performed qualitatively very well and predicted separation in all the four cases as expected. For the Ma = 3.5 cases the separation length varied from 6% to 15% of the isolator length with the increase in the backpressure, and the results compared within 5% of the experiment. For the Ma = 3 case, the separation length was predicted to be 27% of the isolator length, which was 7% larger than those reported in the experiments. The exit Ma was mostly underpredicted, and the errors increased with the separation length, i.e., 2% for the smallest separation length case to 13% for the largest separation length case. For the pressure coefficient, the predictions in the separated flow regime are better than those in the attached flow regime, where the averaged error is 5% and 18%, respectively. The behavior of the MSU model suggests that the model overpredicts pressure compared to the experiment and University of Texas at Arlington 2015 model. The main suspect of such performance is the fact that the MSU model is based on the calorically perfect gas assumption. The University of Texas at Arlington 2015 model, as explained in Chapter 2, is based on the thermally perfect gas assumption. The TPG assumption typically results in temperature lower than the CPG assumption, since not all the energy is used to increase the temperature of the gas. Unlike the calorically perfect gas assumption, the specific heats considered in the TPG assumption are not constant. The quantities are functions of the temperature only. The CPG assumption gets weaker as the temperature register of the application is higher.

CHAPTER V

COMBUSTOR MODEL

5.1   Combustor Model strategy

The burner is a complex station since it involves the combustion of the supersonic flow. The flow changes in this section due to change in area, heat addition, and the occurrence of separation caused by a series of reflected oblique shock waves induced by the pressure rise. It is important to keep in mind that supersonic flow behaves differently than incompressible subsonic flow. On one hand, if the area is increased, the compressible flow accelerates. On the other hand, if heat is added, the supersonic flow decelerates. Taking advantage of these two characteristics is essential to the design of the scramjet engine.

The combustor model is summarized in the figure below:
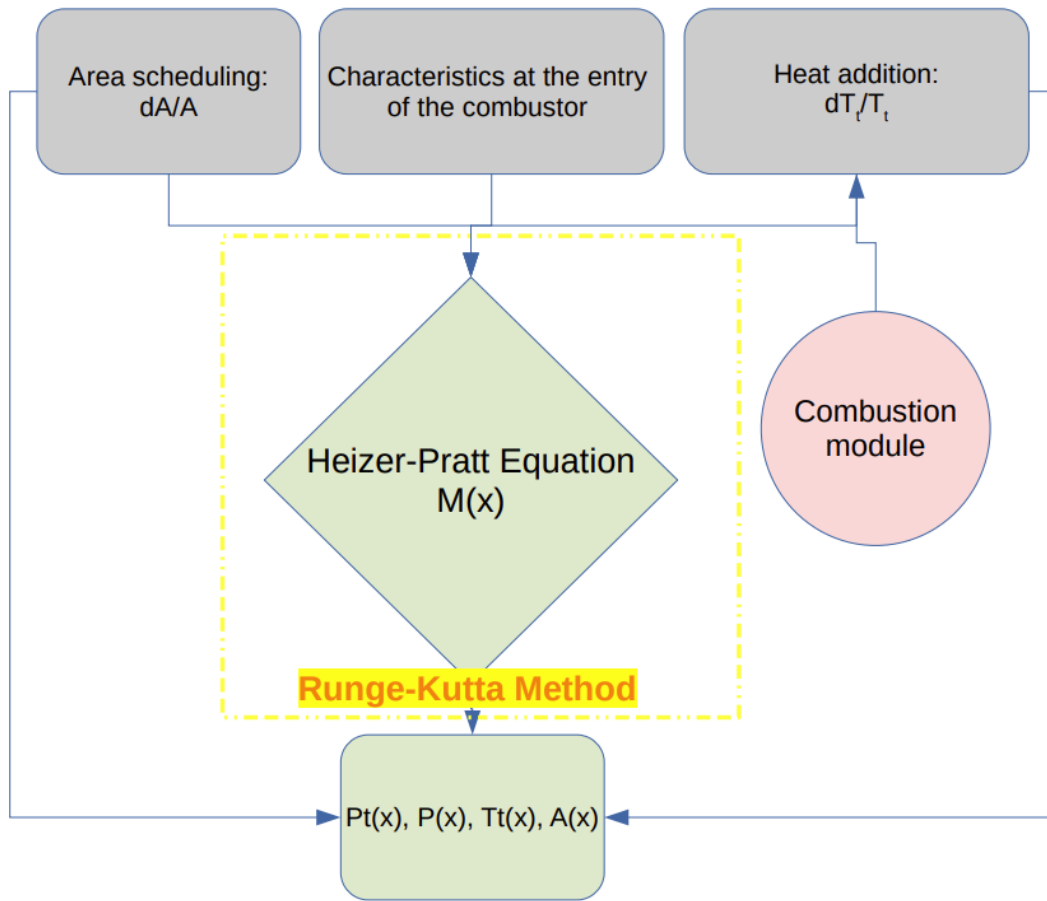
Figure 5.1   Combustor flow Calculations flowchart.

5.2   Heiser-Pratt equations

Ignoring any mass injection, and neglecting friction and wall pressure, among other things, the overall equation according to Heiser and Pratt's [17]:

$$\frac{dM}{dx} = M \frac{\left(1 + \frac{(\gamma - 1)\, M^2}{2}\right)}{1 - M^2}\left[(1 + \gamma M^2)\frac{1}{2}\frac{dT_t}{T_t\, dx} - \frac{1}{A}\frac{dA}{dx}\right] \qquad (5.1)$$

In this section, the heat addition and area change are assumed to have an exponential form. In the next section a better assumption to the area change and heat addition is introduced.

$$\frac{1}{A}\frac{dA}{dx} = C_1$$

41

$$\frac{1}{T_t}\frac{dT_t}{dx} = C_2$$

Where C_1 and C_2 are constants.

Following the same reference [17], the equations for the flow temperature, flow pressure, stagnation pressure, and density are:

$$T(x) = T_3 \frac{T_t(x)}{T_{t3}} \left[\frac{1 + \frac{(\gamma_b - 1)}{2} M_3^2}{1 + \frac{(\gamma_b - 1)}{2} M^2(x)} \right] \tag{5.2}$$

$$P(x) = P_3 \frac{A_3}{A(x)} \frac{M_3}{M(x)} \sqrt{\frac{T(x)}{T_3}} \tag{5.3}$$

$$P_t(x) = P_{t3} \frac{P(x)}{P_3} \left[\frac{T_3}{T(x)} \frac{T_t(x)}{T_{t3}} \right]^{\frac{\gamma}{\gamma-1}} \tag{5.4}$$

$$\rho(x) = \frac{P(x)}{R\,T(x)} \tag{5.5}$$

The stagnation pressure and temperature are identified in the following:

$$T_{t3} = T_3 \left(1 + \frac{(\gamma - 1)}{2} M_3^2 \right)$$

$$P_{t3} = P_3 \left(\frac{T_{t3}}{T_3} \right)^{\frac{\gamma}{\gamma-1}}$$

Given that Eq. 5.1 is a non-linear ODE, the 4th order Runge-Kutta method was applied to solve the equation. The Mach number could be solved in the manner:

$$dM = f(x, M)$$

$$M_{i+1} = M_i + \frac{1}{6} h \left(k_1 + 2k_2 + 2k_3 + k_4 \right)$$

$$k_1 = f(x_i, M_i)$$

$$k_2 = f\left(x_i + \frac{h}{2}, M_i + \frac{hk_1}{2}\right)$$

$$k_3 = f\left(x_i + \frac{h}{2}, M_i + \frac{hk_2}{2}\right)$$

$$k_4 = f(x_i + h, M_i + hk_3)$$

Simultaneously, the area and stagnation temperature are updated according to this discretization:

$$T_{t_{i+1}} = T_{t_i}\,(h\,C_2 + 1)$$

$$A_{i+1} = A_i\,(h\,C_1 + 1)$$

The other parameters are calculated following their respective functions. The boundary

conditions are obtained from the isolator results.

The different cases of the flow within a combustor could be summarized in 4 cases:
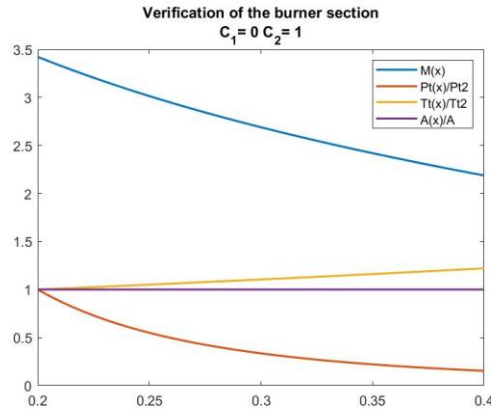
Figure 5.2   Dynamics of Constant Area Burner (CASE 1)
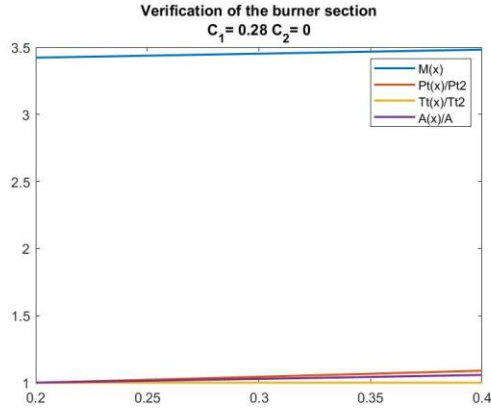
Figure 5.3   Dynamics of a Burner with No Added Heat (CASE 2)
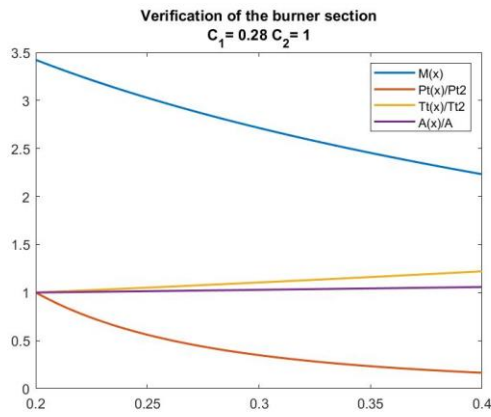
Figure 5.4   Dynamics of a Burner with No Thermal Choke (CASE 3)
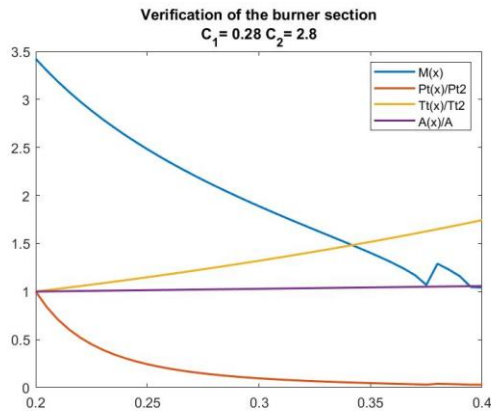
Figure 5.5   Dynamics of a Burner with Thermal Choke (CASE 4)

CASE 1: Keeping the area constant, the added heat is the only parameter affecting the flow. The results suggest that the stagnation pressure and the Mach number are decreasing as the stagnation temperature is increasing. This is coherent with the fact that supersonic flow decelerates as heat is added.

CASE 2: Assuming no heat addition, the area change is the only parameter affecting the flow. The results suggest that the stagnation pressure and the Mach number are increasing as the cross-section area is increasing. This is coherent with the fact that compressible flow accelerates as heat is added.

CASE 3: Both heat addition and area change are included. It is worth noting that the value of the Mach number at the end of this burner, is higher than the one in case 1 (constant area burner). This is because $C_1 > 0$, which means that the area increases, and by consequence, the Mach number is higher.

CASE 4: Thermal choke phenomenon. This occurs when the Mach number is reduced to $M^* = 1$. When Mach number is unity, the problem becomes mathematically undefined. This is due to the existence of the term $1 - M^2$ as a denominator in Eq.10 When $M = 1$, the said term $1 - M^2 = 0$, hence, the presence of oscillations in the plot. To avoid this phenomenon, finding the right combination of $\frac{dT_t}{dx}$ and $\frac{dA}{dx}$ or introducing an area increase at the critical location, are the keys.

5.3   Area Change in the Combustor

A basic combustor model must capture the physics related to the geometry of the machine and the combustion dynamics occurring. Hence, a good approximation for $T_t(x)$ and $A(x)$ is needed to be inputted into the Heiser-Pratt equation.

In real applications, the profile of $A(x)$ is a combination of the geometrical area of the combustor $A_w(x)$, area of the subsonic regions due to separation $A_s(x)$, and the area of the injection wake $A_j(x)$. In other words, $A(x)$ represents the supersonic core flow previously referred to as A_c. $A_s(x)$ depends on the pressure gradient of the flow, while $A_j(x)$ depends on the initial injection area $A_{j,i}$ and the mixing efficiency η_m. In the scope of this work, $A_w(x)$ and $A_s(x)$ are not being considered, which leaves $A(x) = A_w(x)$. For a symmetrical combustor, the area scheduling is written in the form of:

$$d(\ln A) = \ln(A_{x+\Delta x}) - \ln(A_x) \tag{5.6}$$

$$\frac{d(\ln A)}{dx} = \frac{\ln\left(\frac{A_{x+\Delta x}}{A_x}\right)}{dx}$$

For a rectangular cross section area:

$$A_x = a\,D \tag{5.7}$$

$$A_{x+\Delta x} = a\,(D + 2\tan\alpha\ dx) \tag{5.8}$$

For an elliptic cross-section area:

$$A_x = \pi\,a\,\frac{D}{4} \tag{5.9}$$

$$A_{x+\Delta x} = \pi\,a\,\frac{D + 2\tan\alpha\ dx}{4} \tag{5.10}$$

Finally, the area term becomes:

$$\frac{1}{A}\frac{dA}{dx} = \frac{d\ln A}{dx} = \frac{\ln\left(\frac{(D + 2\tan\alpha\ dx)}{D}\right)}{dx} \tag{5.11}$$

46

Where, α is the wall angle entered by the user ranging from $0 \leq \alpha < 90°$. D is the diameter/height of the combustor such that $D = D_{isolator} + 2\,tan\alpha\,(x - x_3)$.

The term dT_t/T_t represents the heat addition. Using the stagnation temperature formula for isentropic flow $T_t(x) = T\left(1 + \frac{\gamma-1}{2}M^2\right)$, the Heiser-Pratt equation could be rewritten as in Eq.5.13.

$$\frac{1}{T_t}\frac{dT_t}{dx} = \frac{dln(T_t)}{dx} = \frac{dln\left(T\left(1 + \frac{\gamma-1}{2}M^2\right)\right)}{dx} = \frac{dln(T)}{dx} + \frac{(\gamma-1)M}{1 + \frac{\gamma-1}{2}M^2}\frac{dM}{dx} \qquad (5.12)$$

$$\frac{dM}{dx} = M\frac{\left(1 + \frac{(\gamma-1)M^2}{2}\right)}{1 - M^2}\left[\frac{(1 + \gamma M^2)}{2}\left(\frac{dln(T)}{dx} + \frac{(\gamma-1)M}{1 + \frac{\gamma-1}{2}M^2}\frac{dM}{dx}\right) - \frac{1}{A}\frac{dA}{dx}\right]$$

$$\frac{dM}{dx} = M\frac{\left(1 + \frac{(\gamma-1)M^2}{2}\right)}{1 - M^2}\frac{(1 + \gamma M^2)}{2}\frac{dln(T)}{dx}$$

$$+ M\frac{\left(1 + \frac{(\gamma-1)M^2}{2}\right)}{1 - M^2}\frac{(1 + \gamma M^2)}{2}\frac{(\gamma-1)M}{1 + \frac{\gamma-1}{2}M^2}\frac{dM}{dx}$$

$$- M\frac{\left(1 + \frac{(\gamma-1)M^2}{2}\right)}{1 - M^2}\frac{1}{A}\frac{dA}{dx}$$

$$\left(1 - M\frac{(\gamma-1)M}{1 - M^2}\frac{(1 + \gamma M^2)}{2}\right)\frac{dM}{dx}$$

$$= M\frac{\left(1 + \frac{(\gamma-1)M^2}{2}\right)}{1 - M^2}\frac{(1 + \gamma M^2)}{2}\frac{dln(T)}{dx} - M\frac{\left(1 + \frac{(\gamma-1)M^2}{2}\right)}{1 - M^2}\frac{1}{A}\frac{dA}{dx}$$

The equation solved in the model is:

$$\frac{dM}{dx} = M \frac{\left(1 + \frac{(\gamma - 1) M^2}{2}\right)}{1 - M^2} \left[\frac{(1 + \gamma M^2)}{2} \frac{dln(T)}{dx} - \frac{1}{A} \frac{dA}{dx}\right] \bigg/ \left(1 - M \frac{(\gamma - 1)M}{1 - M^2} \frac{(1 + \gamma M^2)}{2}\right) \tag{5.13}$$

Since the area scheduling has been already determined as discussed in this section, the only unknown in the Eq. 5.13 is the term $\frac{dln(T)}{dx}$. Indeed, T is thermodynamic temperature, which in this case is the presentative of the combustion effect. Hence, the quantification of $T(x)$ is approximated in the combustion module.

5.4   Combustion Module

If a combustion of equivalence ratio Φ takes place within the combustion, it is noticed that not all the fuel reacts with the oxidizer instantly. In other words, as the flow advances, the fuel is getting mixed with the oxidizer. Hence, the combustion happens in accordance with the reactant equivalence ratio ϕ_r such that, as $x \sim L_{mix}$, $\phi_r \sim \Phi$ [3]. Following this fact, an estimation of $\phi_r(x)$ could be the key to estimate the term $T(x)$.
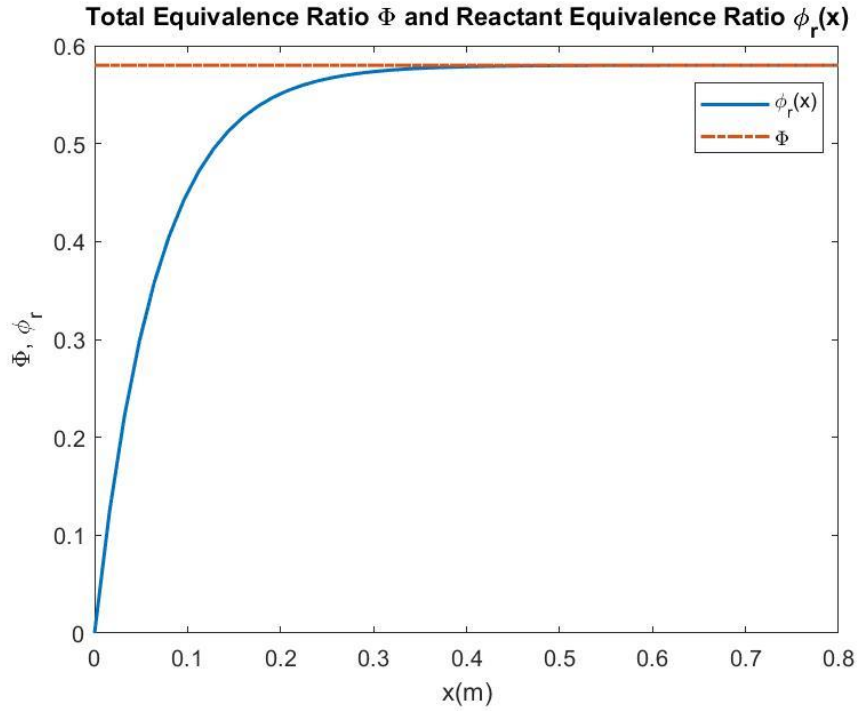
Figure 5.6   Change of $\phi_r(x)$ and Φ .

The reactant equivalence ratio is,

$$\phi_r = \frac{\dfrac{Y_F}{Y_{Ox}}}{\left.\dfrac{Y_F}{Y_{Ox}}\right|_{st}} \tag{5.14}$$

Where, Y_F and Y_{ox} are the mass fractions of the mixed fuel and oxidizer respectively, and $\left.\dfrac{Y_F}{Y_{Ox}}\right|_{st}$ is the fuel-to-oxidizer mass fraction ratio in a stoichiometric configuration.

A useful parameter often used in non-premixed combustion applications is the mixing efficiency η_m. Indeed, ensuring the mixing of the fuel and oxidizer on a molecular level has been a subject of interest in combustion research. Fortunately, current literature has provided many empirical formulas of η_m for many types of injections (perpendicular injection, parallel wall

49

injection, strut injection, ramp injection…). The definition of the mixing efficiency could be simplified into [3]:

$$\eta_m = \frac{\phi_r}{\Phi}$$ (5.15)

Finally,

$$\phi_r(x) = \Phi \, \eta_m(x)$$ (5.16)

The profile of $\eta_m(x)$ varies with the injection properties as indicated previously. The mixing could be linear or dependent on other parameters. The formula used for this code is general correlation:

$$\eta_m(x) = 1 - e^{-\frac{\ln(1-\eta_{max})}{L_{mix}}(x-x_c)}$$ (5.17)

Where, η_{max} is the maximum efficiency and L_{mix} is the mixing length. In [17], it is stated: "a mixing length of 20 cm. and maximum mixing efficiency of 95% may constitute a typical mixing definition". Hence, the default values of η_{max} and L_{mix} are fixed to be 95% and 0.2cm respectively. Though, the user may change those values to test different configurations.

The next task is to select a thermodynamic approach to model the temperature profile based on the obtained $\phi_r(x)$. One of the simplest concepts one may incorporate is the adiabatic flame concept. An adiabatic flame implies that all the heat generated in the combustion is used to heat the products instead of exchanging it to the surroundings.[25] Assuming chemical equilibrium conditions, no heat transferred to the walls, and complete combustion:

$$h_{react}(T_3, P_3) = h_{prod}(T_{ad}, P_3) \tag{5.18}$$

Or,

$$h_{burnt}(T_3, P_3) = h_{unburnt}(T_{ad}, P_3) \tag{5.19}$$

The mixture enthalpy is given by,

$$h_{mix} = \sum_{n}^{N} Y_n \, h_n \tag{5.20}$$

Where Y_n and N indicate the mass fraction of the nth species and total number of species, respectively.

To get the enthalpy of mixture, one must find Y_n and $H_n(T)$.

First, for the unburnt mixture:

$$Y_F = \frac{X_{ox} \, \phi_r(x)}{\upsilon_{ox,r}} \, \upsilon_{F,r} \frac{MW_F}{MW_{mix}} \tag{5.21}$$

$$Y_{Ox} = X_{Ox} \frac{MW_{ox}}{MW_{mix}} \tag{5.22}$$

$$Y_{Pr} = 0 \tag{5.23}$$

Where, X represents the mass fraction, $\upsilon_{n,r}$ is the reaction coefficient of the species in the chemical combustion.

For the burnt mixture:

$$\frac{dY_1}{\upsilon_{1,s}\ MW_1} = \frac{dY_2}{\upsilon_{2,s}\ MW_2} = \cdots for\ all\ species \tag{5.24}$$

Where, $\upsilon_{n,s}$ is the stoichiometric coefficient of the species.

$$\frac{\left(Y_{F,b} - Y_{F,u}\right)}{\upsilon_{F,s}\ MW_F} = \frac{\left(Y_{ox,b} - Y_{ox,u}\right)}{\upsilon_{ox,s}\ MW_{ox}} = \frac{\left(Y_{Pr,b} - Y_{Pr,u}\right)}{\upsilon_{Pr,s}\ MW_{Pr}} \tag{5.25}$$

$$\begin{cases} Y_{F,b} = 0 & \phi_r(x) < 1 \\ Y_{ox,b} = 0 & \phi_r(x) > 1 \\ Y_{F,b} = Y_{ox,b} = 0 & \phi_r(x) = 1 \end{cases} \tag{5.26}$$

The temperature relation could be extracted from,

$$h_{mix}(T) - h_{ref} = \int_{T_{ref}}^{T} c_p\ dT \tag{5.27}$$

Finally, c_p and $h(T)$ are calculated using NASA polynomials [15].

Once all the mathematical equations are set, the work plan to find the temperature profile $T(x)$ is summarized in the following:
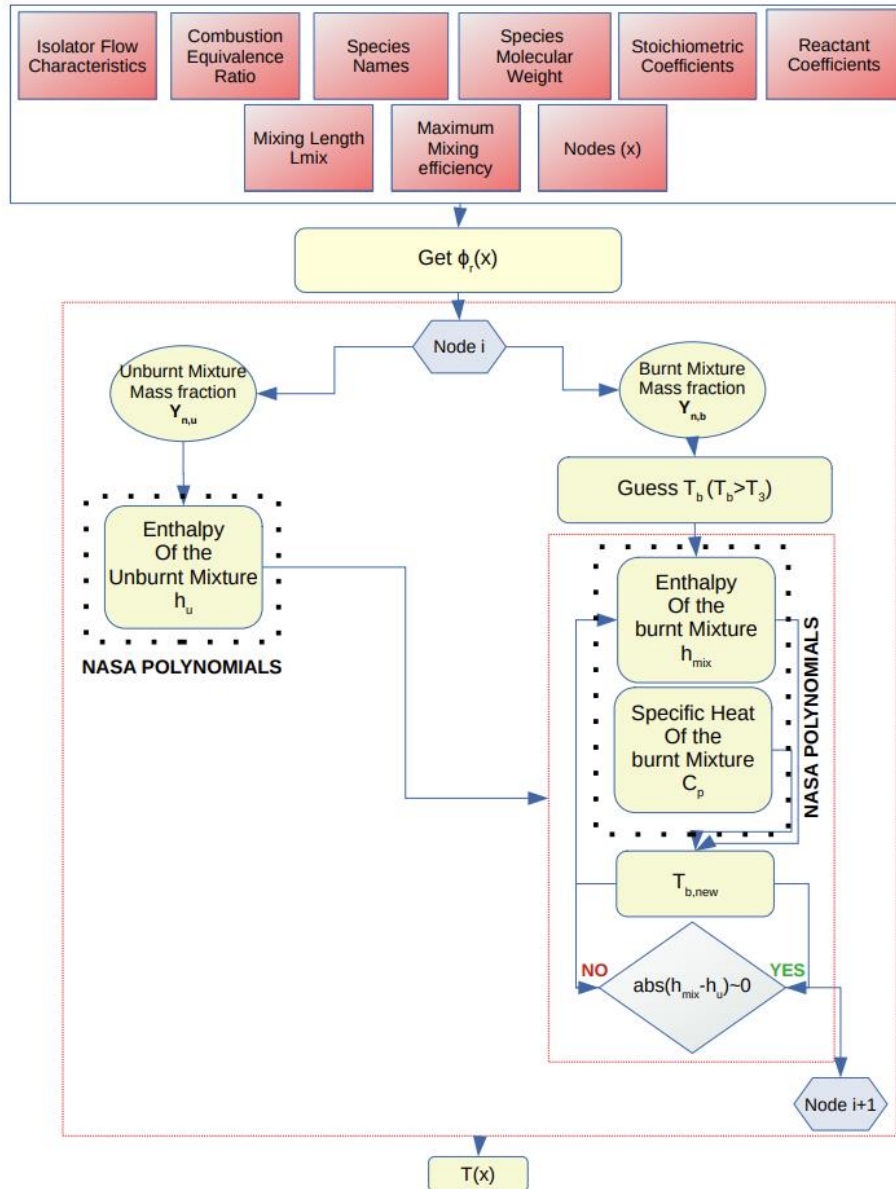
Figure 5.7   Combustion Module schematic

5.5   Combustor Validation

The setup of R. R. Boyce experiment is shown in the figure below. Hydrogen fuel is injected sonically into the incoming air. The combustor entry conditions were borrowed from [10]. Indeed, the values used are $M_3 = 2.47$, $P_3 = 59000\ Pa$, and $T_3 = 1025\ K$. The goal of this

verification is to evaluate the performance of the MSU to experimental data and more accurate

analytical models with more elaborate and detailed combustion codes. While the models of the

University of Texas at Arlington use the mixing efficiency model for a strut injection of

Hydrogen fuel, the efficiency model presented in this paper is used in this verification. The

purpose is to assess the importance of the mixing profile on scramjet modelling.
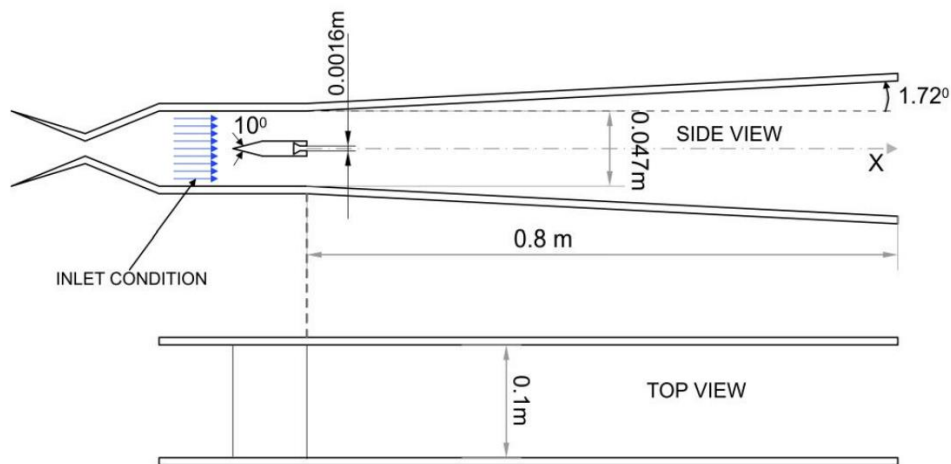
Figure 5.8   Dimensions of the combustor used in Boyce Experiment [10].

The results of the MSU combustion model are presented below for $\Phi = 0.19$, $\Phi = 0.38$,

and $\Phi = 0.58$.
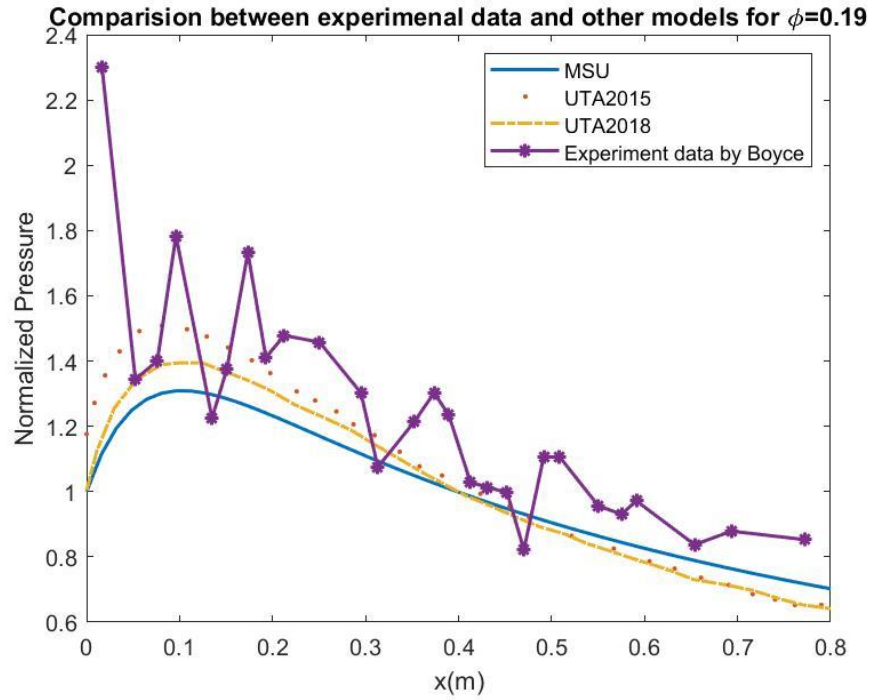
Figure 5.9   Normalized Pressure Profile for Combustor Verification for $\Phi = 0.19$.
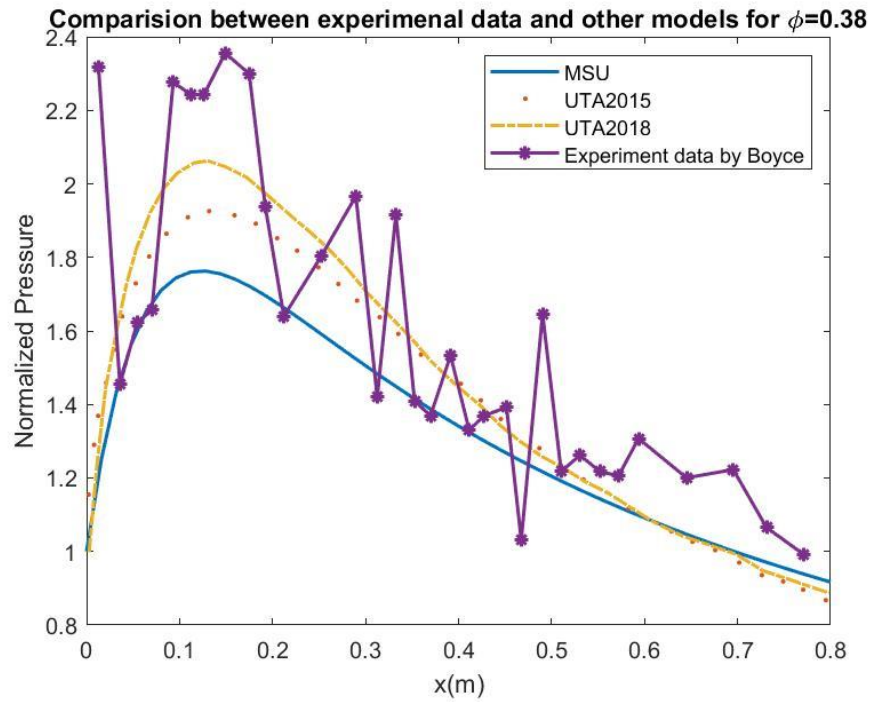
Figure 5.10   Normalized Pressure Profile for Combustor Verification for $\Phi = 0.38$.
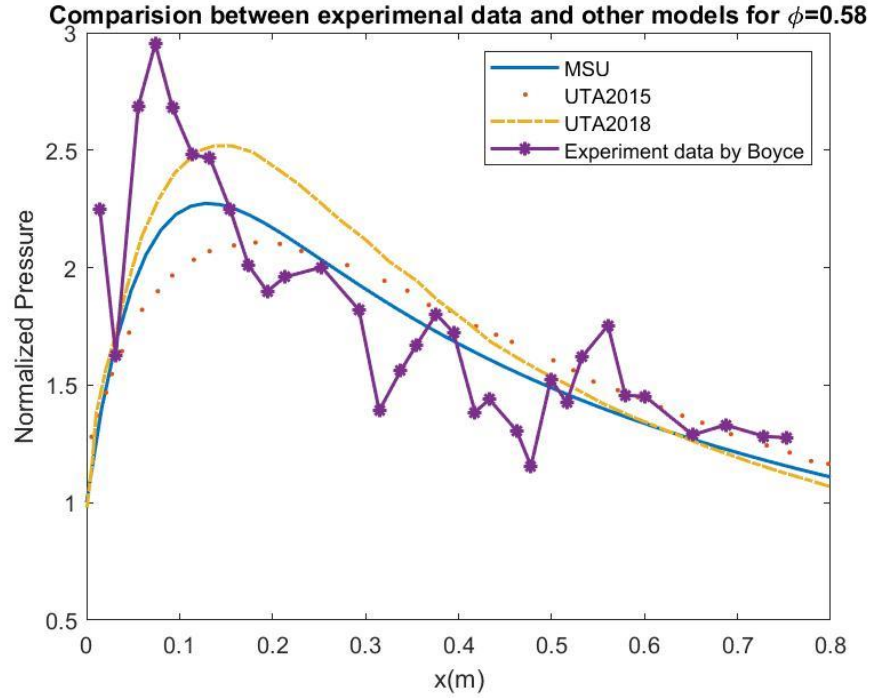
Figure 5.11   Normalized Pressure Profile for Combustor Verification for $\Phi = 0.58$.

It is apparent from the results that MSU code underpredicts the pressure compared to the provided references. The main suspect of the underprediction is the area profile $A(x)$. Indeed, the $A(x)$ values calculated in the MSU model are higher than the ones used in the analytical models of the University of Texas at Arlington. Both reference models at least include the area change due to the jet injection, the geometry of the strut… As explained previously, $A(x)$ is the result of the subtraction of jet area profile $A_j(x)$ and the area of the induced subsonic regions $A_s(x)$ from the wall area $A_w(x)$.

The verification results are done by assuming the mixing profile presented the section 5.3. To examine the effect of the mixing length on the performance of the model, the mixing length was set $L_{mix} \sim 0.85$.
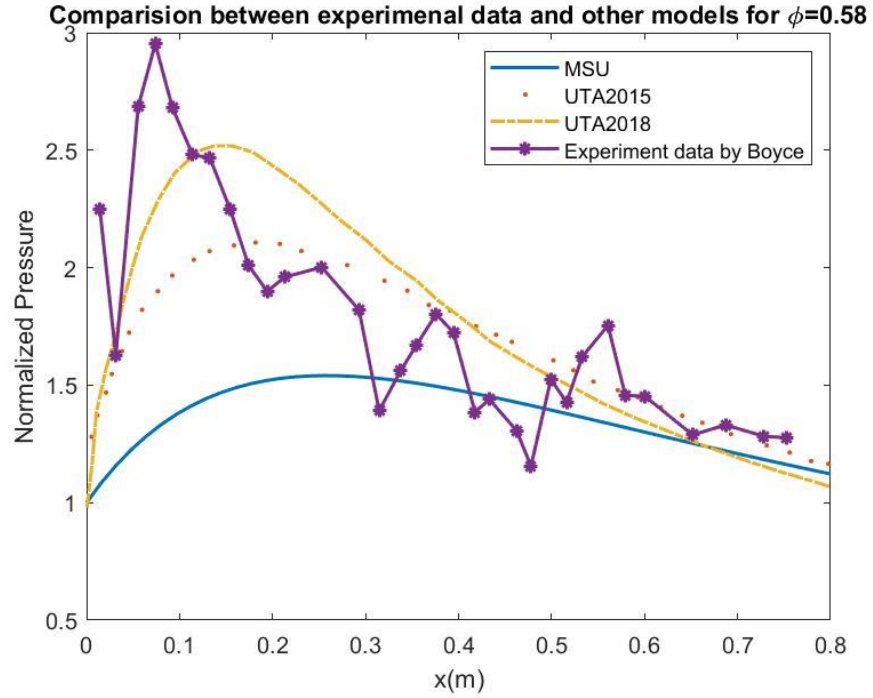
Figure 5.12   Normalized Pressure Profile for $L_{mix} = 0.8518$

Using the empirical formula for Hydrogen strut injector as presented in Eq. 5.12 [10] The following results were found:

$$\eta_{m,H_2\ strut} = 1.06492 \left(1 - e^{-\left(3.69639\frac{x}{L_{mix}}\right)^{0.80586}}\right)$$

(5.28)

For $L_{mix} = 0.2$:
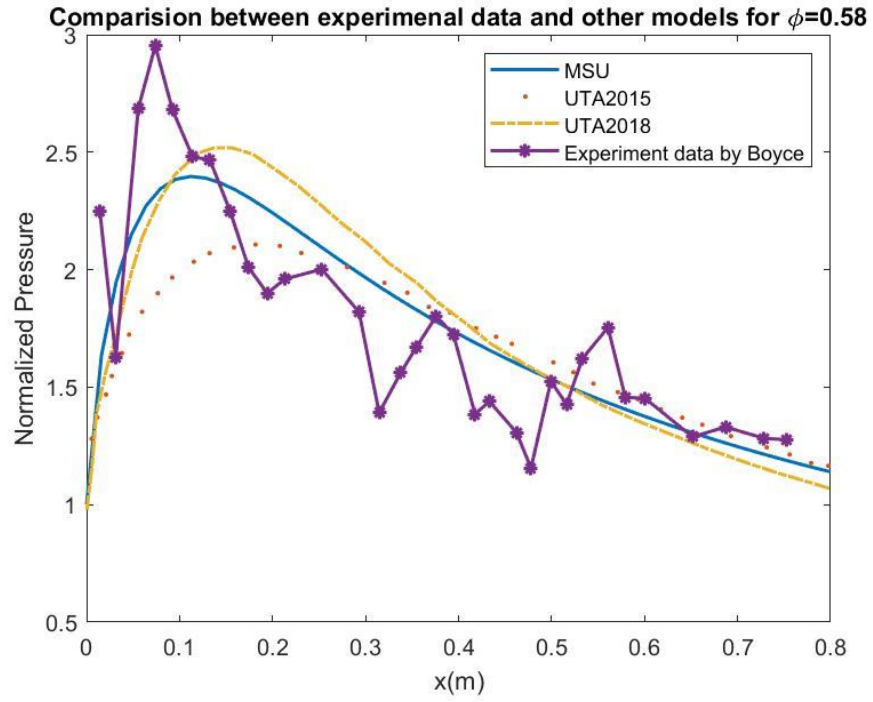
Figure 5.13   Normalized Pressure Profile for Strut Hydrogen Injector Mixing Model with $L_{mix} = 0.2$

For $L_{mix} = 0.8518$:
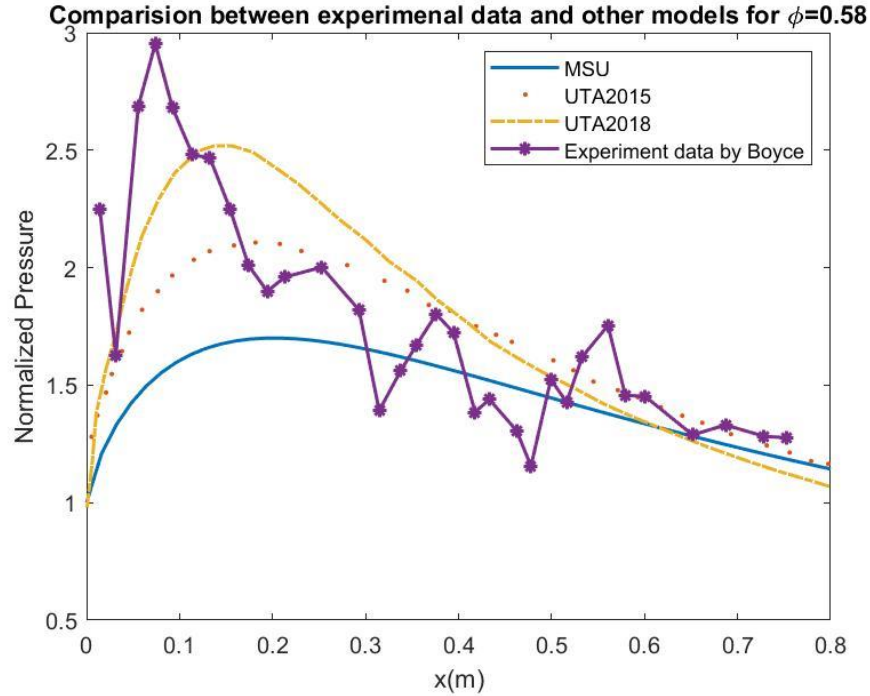
Figure 5.14   Normalized Pressure Profile for Strut Hydrogen Injector Mixing Model with $L_{mix} = 0.8518$

It is clear from the results that the mixing parameters are critical in the scramjet modelling. A lower mixing efficiency length typically results in a steeper pressure profile. Indeed, if the fuel is totally mixed at distance closer to the injector, the overall combustion happens closer to the combustion chamber entry. The cross-section area near the entry of the combustor is smaller than at the exit. Hence, it could be deduced that the overall heat addition for small mixing lengths happens in cross-section areas relatively smaller than the cross-section areas of larger mixing lengths. Given that heat addition decelerates compressible flows while area increase accelerates the fluid, it apparent why the pressure rise for $L_{mix} = 0.2$ is higher than $L_{mix} = 0.8518$ case.

CHAPTER VI

COMBUSTOR-ISOLATOR INTERACTION

6.1   Changes within the combustor

As foreshadowed previously, the incoming flow to the combustor is attached. The model

calculates the Mach number, pressure, temperature, and density profiles following the strategy

presented in Chapter 5. Following this task, the model locates the highest pressure P_{cmax} and

evaluates the ratio M_{cmax}/M_3. If the empirical criterion for turbulent flows $\frac{M_{cmax}}{M_3} < 0.762$ is

satisfied, the flow's boundary layer is assumed to separate. Once the existence of separation has

been confirmed, the flow is assumed to adjust itself such that, the pressure remains constant from

the injector to the location x_{cmax} at P_{cmax}. Neglecting wall friction, the differential $\frac{du^2}{u^2}$ is zero of

constant pressure according to the momentum conservation equation. The Mach number is then

obtained:

$$\frac{dM}{dx} = -\frac{M}{2}\frac{dlnT}{dx}$$

(6.1)

The entire procedure could be summarized in the following figure:
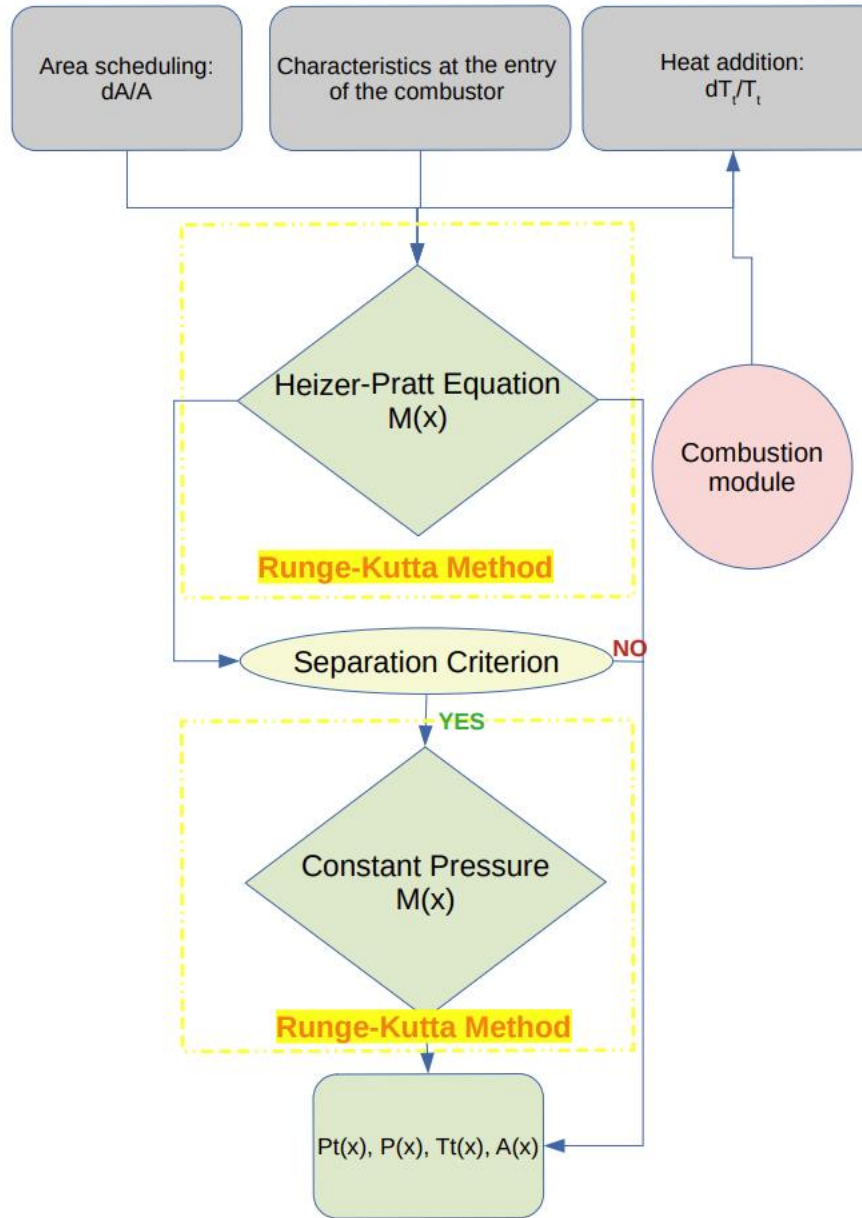
Figure 6.1   Combustor model summary

6.2   Changes within the isolator

Once the flow within the combustor has been adjusted and the new pressure at the isolator entry has been obtained such that, $P_{3,new} = P_{cmax}$, the flow within the isolator is reevaluated according to the flowchart below. From this section onwards, P_3 corresponds to the new isolator exit pressure, unless stated otherwise.
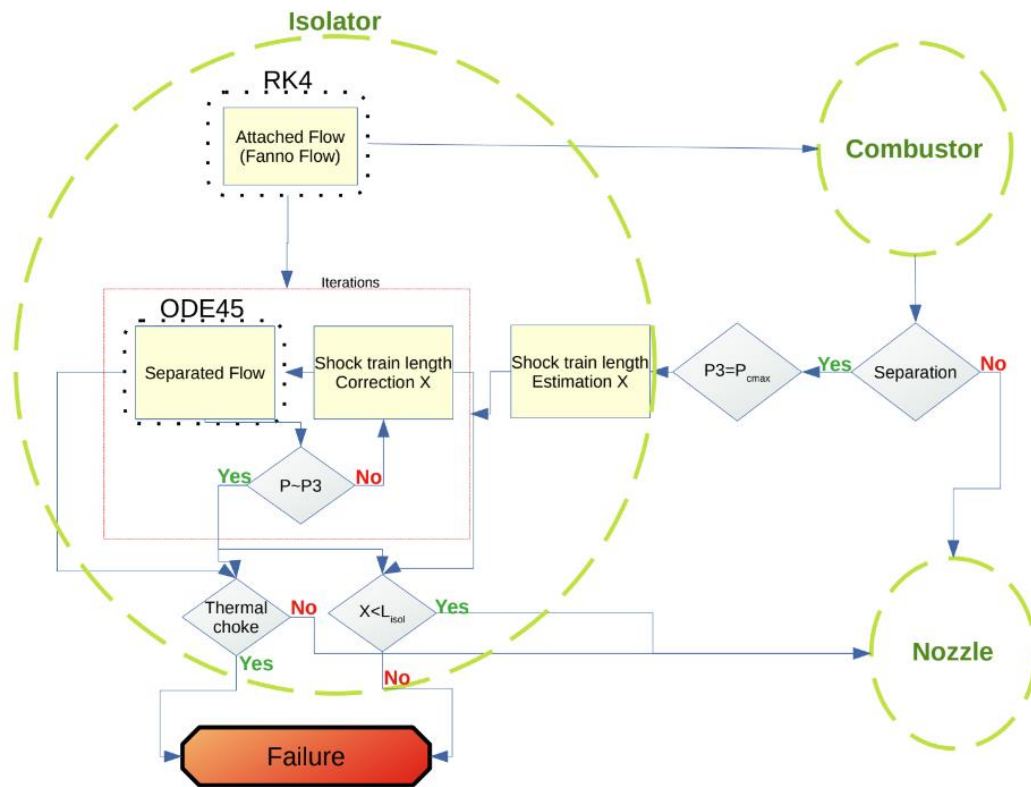
Figure 6.2   Isolator model summary

First, the flow is divided into two regions: attached flow and detached flow. The first

estimation of the length of the detached flow is obtained from shock train length correlation

Hence, the initial estimation of the separation point is $x_u = x_3 - X_{shock}$. Due to the inaccuracy

of the correlation, the solution gives a mismatch between the pressure calculated at the end of the

isolator and P_3. Afterward, the model keeps iterating while changing X_{shock} until $P(x_3) \sim P_3$.

CHAPTER VII

MODEL SUMMARY

The Algorithm of the MSU model is summarized in the figure below:
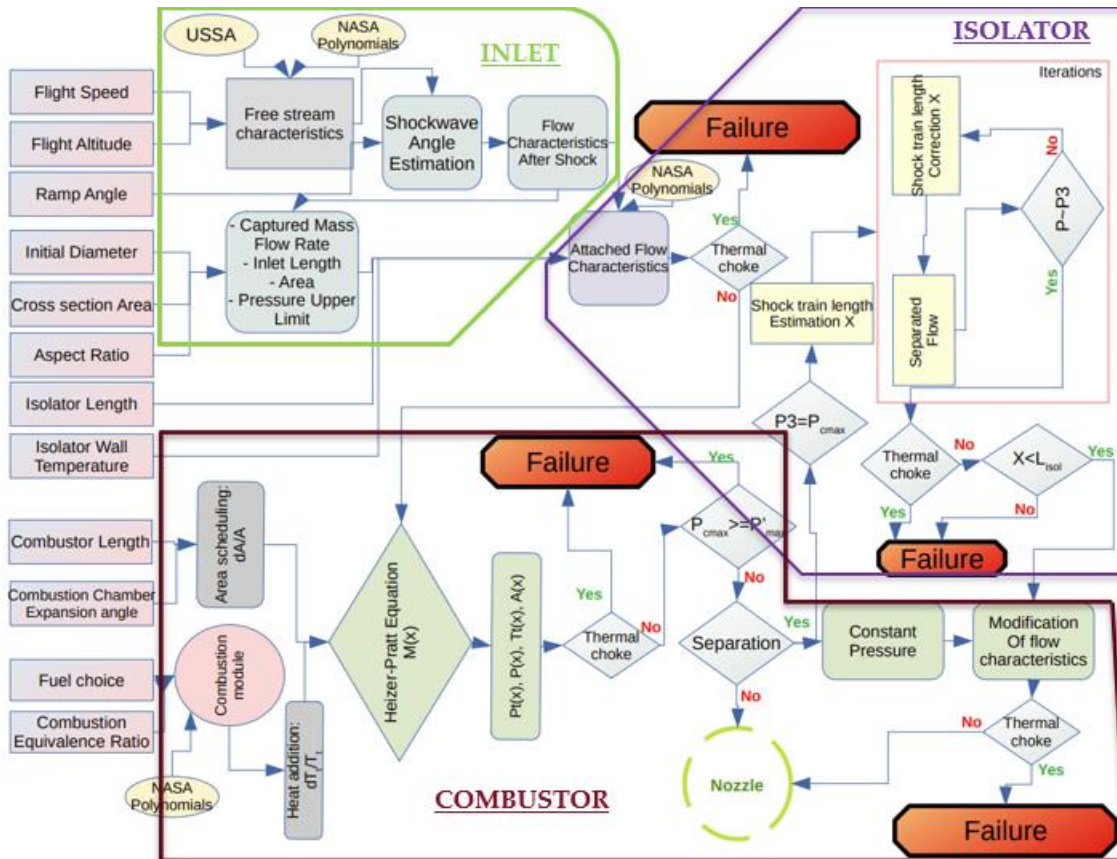
Figure 7.1   Flowchart summarizing the operation flow of the MSU model.

The model allows the user to enter about 12! possible combinations to analyze. When the user's configuration results into a functioning scramjet, the model plots the flow characteristics throughout the scramjet in the following manner:
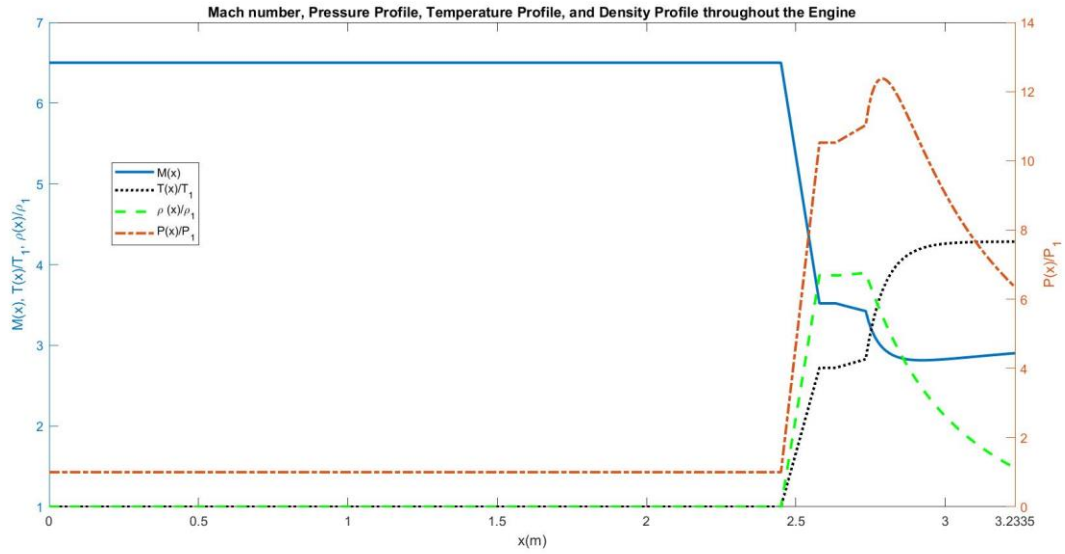
Figure 7.2   An example of the output of the MSU model for functioning scramjet
configuration with no separation.

In addition of plotting all the four thermodynamics characteristics with respect to x (the length of

the scramjet), the model prompts the user to write the findings in a .cvs file. If the scramjet

functions, but separation was predicted, the model displays the shock-train length to the user. An

example of a plot with separation is shown:
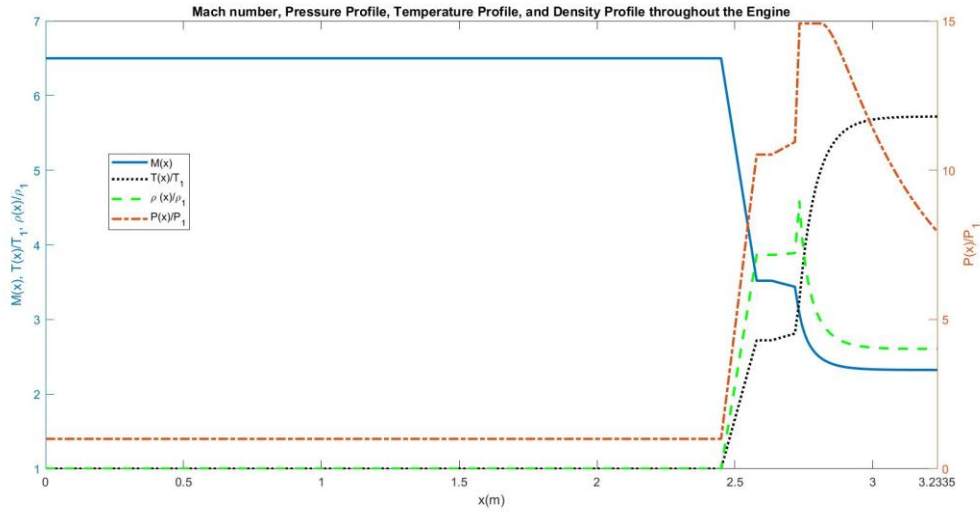
Figure 7.3   An example of the output of the MSU model for functioning scramjet configuration with separation.

In case of failure, the plots for thermal choke are done similarly as the other plots and the failure is announced. However, in case of long shock train, changes are done to the calculated values. Indeed, the long shock train implicitly hints that counter flow that have reached the inlet, which further implies that no flow is entering the engine. Hence, The Mach number is set to zero starting the inlet's throat. Then, pressure and density are set to equal the maximum pressure and density starting the same location. The temperature is indicated by setting the isolator's calculated exit temperature at the inlet's exit and setting the combustor's maximum temperature at the at the isolator exit. Certainly, those changes do not represent the real flow thermodynamic values, but these actions are necessary to provide an insight on what caused the shock train. Hence, values like maximum pressure and temperature are recorded. An example of a flow plot with a failure due to long shock train is presented below:

65
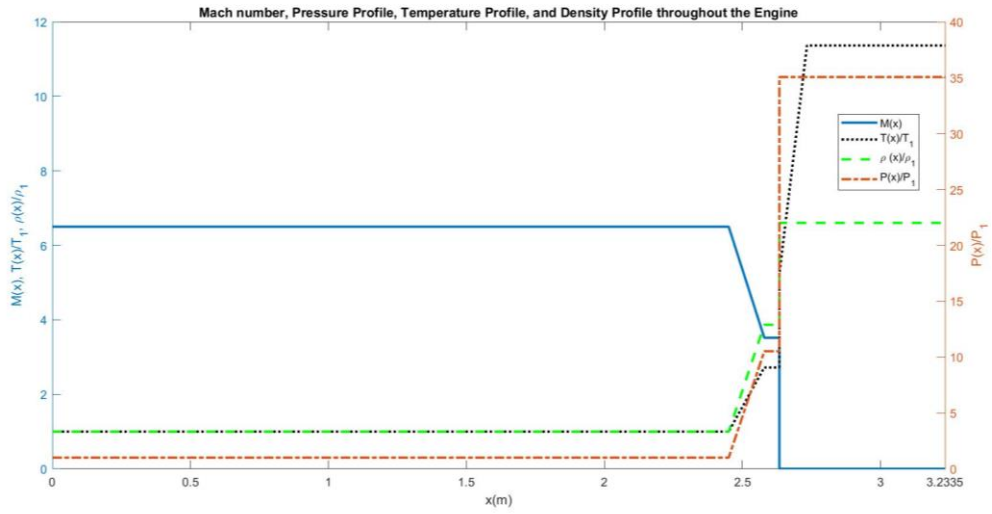
Figure 7.4   An example of the output of the MSU model for failed scramjet configuration with a long shock train.

CHAPTER VIII

ANALYSIS OF THE SCRAMJET ENGINE USING THE PROPOSED MODEL

8.1 Tests ran and Objectives

After the model had been developed and validated, a parametric study has been performed to highlight some trends and insights of the scramjet engine. While the model enables the user to run a large number of combinations, only five tests are selected in this work. The tests are summarized in the table below:

Table 8.1   Summary of the tests done in the scope of the parametric analysis

TEST:	Objective:	Action
I	Investigating the effect of equivalence ratio on the scramjet functioning.	Incrementing the combustion equivalence ratio by 0.01 and record the cases where 1st separation appears, and 1st failure appears
II	Investigating the effect of the fuel type on the scramjet flow.	Incrementing the combustion equivalence ratio by 0.01 and record the cases where 1st separation appears, and 1st failure appears for kerosene C_2H_4 and comparing it with Hydrogen H_2.
III	In Investigating the effect of the flight speed on the scramjet functioning.	Modify the Mach number of the flight conditions of TEST I with $\Phi = 0.1$ and record the first appearance of failure and separation.
IV	Investigating the effect of combustion chamber size on the scramjet functioning.	Setting a lower and higher expansion angle $\alpha = 1°$, $\alpha = 3°$, and $\alpha = 6°$ for flight conditions similar to TEST I with $\Phi = 0.1$
V	Investigating the effect of a shorter isolator for a flow with separation on the scramjet functioning	For a flight conditions similar to TEST I with a flight Mach number $M_1 = 5$ and with $\Phi = 0.45$ and record the 1st failure cases for the bounds of the isolator length.

8.2 Results and Discussion

The configurations obtained from the first test and the results are summarized below:

Table 8.2 Configurations obtained from TEST I

TEST I					
User's Input Parameters	Case	No combustion	Attached flow	Separation	Failure
	Flight Mach Number:	6.5	6.5	6.5	6.5
	Flight Altitude in m:	20,000	20,000	20,000	20,000
	Ramp Angle θ in degrees:	20	20	20	20
	Intake Height/Diameter in m:	1	1	1	1
	Aspect Ratio:	2	2	2	2
	Rectangular or Elliptic Cross section:	Rectangular	Rectangular	Rectangular	Rectangular
	Isolator Length in m:	0.1	0.1	0.1	0.1
	Isolator Wall Temperature in K:	300	300	300	300
	Combustion Chamber Expansion angle α in degrees:	3	3	3	3
	Combustor Length in m:	0.5	0.5	0.5	0.5
	Fuel Choice:	H_2	H_2	H_2	H_2
	Combustion Equivalence Ratio Φ:	0	0.1	0.17	0.8

Table 8.3   Results obtained from TEST I

		TEST I			
	Case	No combustion	Attached flow Φ = 0.1	Separation Φ = 0.17	Failure Φ = 0.8
	Shock Train Length with respect to isolator length:	0	0	16%	99%
	Failure Nature	-	-	-	Long Shock Train
Results	Mach Number Profile				

Mach Number Profile throughout the Engine for TEST I for Φ=0, Φ=0.1, Φ=0.18, and Φ=0.8

| Pressure Profile |

Pressure Profile throughout the Engine for TEST I for Φ=0, Φ=0.1, Φ=0.18, and Φ=0.8

| Temperature Profile |

Temperature Profile throughout the Engine for TEST I for Φ=0, Φ=0.1, Φ=0.18, and Φ=0.8

69

It is noticeable how the flow is decelerated as the equivalence ratio is increasing. The maximum temperature a chemical reaction can produce is in stoichiometric conditions, in other words, when $\Phi = 1$. Hence, as the equivalence ratio is approaching unity, the temperature produced is higher, which leads to a further deceleration of the flow and a higher pressure rise. In the no combustion case, the flow is slightly accelerated due to the no heat addition and area expansion. The pressure rise in case $\Phi = 0.8$ was quite large to be contained by the isolator. Some "remedies" to this failure case are designing a scramjet with a longer isolator or smaller ramp angle. A longer isolator will be able to contain the shock train. A smaller ramp angle will produce a weaker compression, thus, a smaller isolator entry Mach number, which implies that the flow has more momentum to counter the pressure rise. However, it is imperative to note that the suggested "remedies" should be selected based on analysis as more problems may emerge.
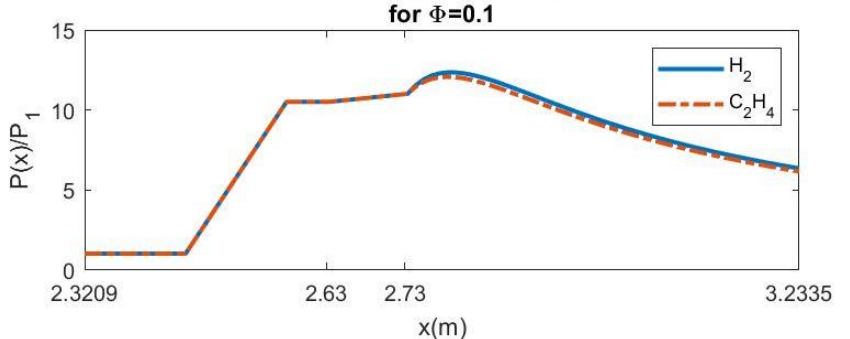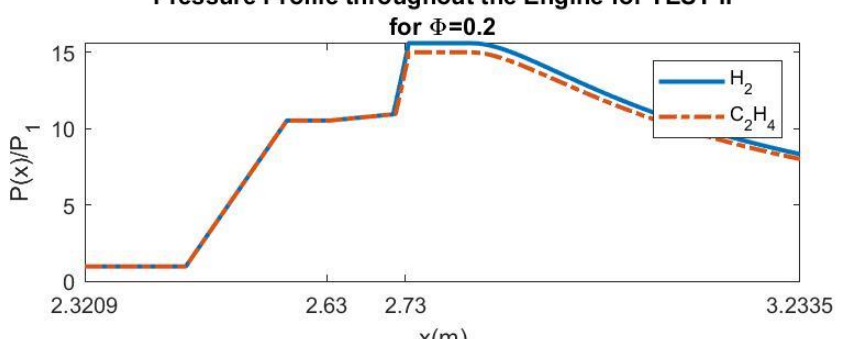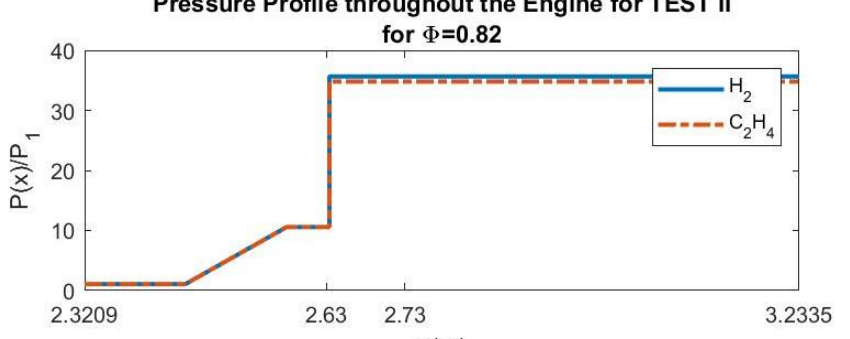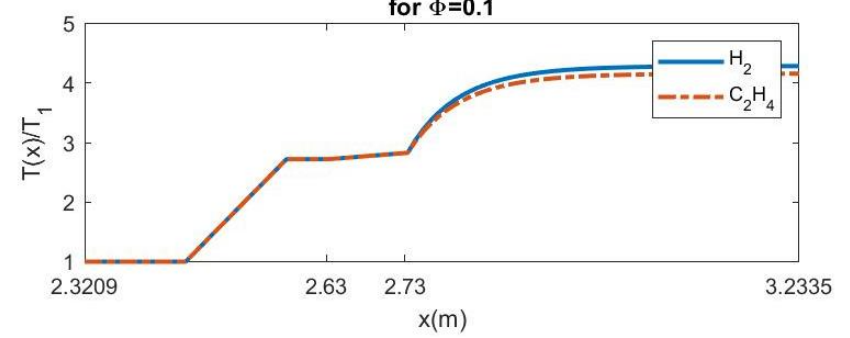
The next study highlights the effect of the fuel type. First, a summary of the configurations used in TEST II as well as the results obtained:

Table 8.4   Configurations obtained from TEST II

	TEST II			
	Parameter:	Attached Flow	Separation	Failure
	Flight Mach Number:	6.5	6.5	6.5
	Flight Altitude in m:	20,000	20,000	20,000
	Ramp Angle θ in degrees:	20	20	20
	Intake Height/Diameter in m:	1	1	1
	Aspect Ratio:	2	2	2
User's Input Parameters	Rectangular or Elliptic Cross section:	Rectangular	Rectangular	Rectangular
	Isolator Length in m:	0.1	0.1	0.1
	Isolator Wall Temperature in K:	300	300	300
	Combustion Chamber Expansion angle α in degrees:	3	3	3
	Combustor Length in m:	0.5	0.5	0.5
	Fuel Choice:	C_2H_4	C_2H_4	C_2H_4
	Combustion Equivalence Ratio Φ:	0.1	0.2	0.82

Table 8.5　　　　Results obtained from TEST II

		Case	Attached flow $\Phi = 0.1$	Separation $\Phi = 0.2$	Failure $\Phi = 0.82$
Results		Shock Train Length with respect to isolator length:	0	13.4%	99%
		Failure Nature	-	-	Long Shock Train
	Mach Number				

Mach Number Profile throughout the Engine for TEST II for $\Phi=0.1$

Mach Number Profile throughout the Engine for TEST II for $\Phi=0.2$

Mach Number Profile throughout the Engine for TEST II for $\Phi=0.82$

	Pressure	**Pressure Profile throughout the Engine for TEST II for Φ=0.1** **Pressure Profile throughout the Engine for TEST II for Φ=0.2** **Pressure Profile throughout the Engine for TEST II for Φ=0.82**
	Temperature	**Temperature Profile throughout the Engine for TEST II for Φ=0.1**

Temperature Profile throughout the Engine for TEST II for $\Phi=0.2$

Temperature Profile throughout the Engine for TEST II for $\Phi=0.82$

Both chosen fuels are heavily used for scramjet studies. As it is showcased by the plots, Hydrogen leads to higher pressure compared to Kerosene. This due to the higher adiabatic flame the Hydrogen produces compared to Kerosene. It is also why Kerosene has a wider interval of equivalence ratio compared to Hydrogen. The fuel selection still needs to take into consideration the ignition time of both fuels. Indeed, aside from having a higher adiabatic flame temperature, the Hydrogen also holds the advantage of a faster ignition time. That's why, it is often used in faster flight speeds instead of using conventional hydrocarbons.

Similarly, information and findings of the third test are summarized as follows.

Table 8.6   Configurations obtained from TEST III

TEST III					
User's Input Parameters	Parameter:	Attached Flow	Separation	Failure
	Flight Mach Number:	10	4.2	3.1
	Flight Altitude in m:	20,000	20,000	20,000
	Ramp Angle θ in degrees:	20	20	20
	Intake Height/Diameter in m:	1	1	1
	Aspect Ratio:	2	2	2
	Rectangular or Elliptic Cross section:	Rectangular	Rectangular	Rectangular
	Isolator Length in m:	0.1	0.1	0.1
	Isolator Wall Temperature in K:	300	300	300
	Combustion Chamber Expansion angle α in degrees:	3	3	3
	Combustor Length in m:	0.5	0.5	0.5
	Fuel Choice:	H_2	H_2	H_2
	Combustion Equivalence Ratio Φ:	0.1	0.1	0.1

Table 8.7   Results obtained from TEST III

TEST III				
	CASE	Attached Flow $M_1 = 10$	Separation $M_1 = 4.2$	Failure $M_1 = 3.1$
	Shock Train	0	33%	99.9%
Results	Failure Nature	-	-	Long Shock Train
	Mach Number	**Mach Number Profile throughout the Engine for TEST III** for M_1=3.1, M_1=4.2, and M_1=10; M(x) vs x(m); legend: M_1=3.1, M_1=4.2, M_1=10		
	Pressure	**Pressure Profile throughout the Engine for TEST III** for M_1=3.1, M_1=4.2, and M_1=10; P(x)/P$_1$ vs x(m); legend: M_1=3.1, M_1=4.2, M_1=10		
	Temperature	**Temperature Profile throughout the Engine for TEST III** for M_1=3.1, M_1=4.2, and M_1=10; T(x)/T$_1$ vs x(m); legend: M_1=3.1, M_1=4.2, M_1=10		

76

In this case, it is proven that the same scramjet configuration may lead to different results for different flight speeds. This behavior is due to difference in momentum the flow has at it enters the isolator. If the Mach number at the entry of the isolator is lower, the Mach number at the combustor entry will lower. In other words, the flow has less momentum to counter the flow rise. It is also worthy to note that mass flow rate decreases as the Mach number gets lower. Finally, it noticeable that the temperature and pressure are relatively higher as the Mach number gets higher. This explained by the direct proportionality with the Mach number in the bow shock equation.

Table 8.8   Configurations obtained from TEST IV

TEST IV				
	Parameter:	Attached Flow	Separation	Separation
	Flight Mach Number:	6.5	6.5	6.5
	Flight Altitude in m:	20,000	20,000	20,000
	Ramp Angle θ in degrees:	20	20	20
	Intake Height/Diameter in m:	1	1	1
	Aspect Ratio:	2	2	2
User's Input Parameters	Rectangular or Elliptic Cross section:	Rectangular	Rectangular	Rectangular
	Isolator Length in m:	0.1	0.1	0.1
	Isolator Wall Temperature in K:	300	300	300
	Combustion Chamber Expansion angle α in degrees:	6	3	1
	Combustor Length in m:	0.5	0.5	0.5
	Fuel Choice:	H_2	H_2	H_2
	Combustion Equivalence Ratio Φ:	0.17	0.17	0.17

Table 8.9   Results obtained from TEST IV

Text IV				
	CASE	Attached Flow $\alpha = 6°$	Separation $\alpha = 3°$	Separation $\alpha = 1°$
	Shock Train	0	16%	27%
	Failure Nature	-	-	Long Shock Train
Results	Mach Number			
	Pressure			
	Temperature			

Mach Number Profile throughout the Engine for TEST IV for $\alpha=1°$, $\alpha=3°$, and $\alpha=6°$

Pressure Profile throughout the Engine for TEST IV for $\alpha=1°$, $\alpha=3°$, and $\alpha=6°$

Temperature Profile throughout the Engine for TEST IV for $\alpha=1°$, $\alpha=3°$, and $\alpha=6°$

It is noticed that as the expansion angle gets lower, the pressure rise gets higher. Since pressure is inversely proportional to the area, this behavior is expected.

78

Table 8.10   Results obtained from TEST V

TEST V					
User's Input Parameters	Parameter:	Failure	Separation	Failure	
	Flight Mach Number:	5	5	5	
	Flight Altitude in m:	20,000	20,000	20,000	
	Ramp Angle θ in degrees:	20	20	20	
	Intake Height/Diameter in m:	1	1	1	
	Aspect Ratio:	2	2	2	
	Rectangular or Elliptic Cross section:	Rectangular	Rectangular	Rectangular	
	Isolator Length in m:	0.14	0.2	1	
	Isolator Wall Temperature in K:	300	300	300	
	Combustion Chamber Expansion angle α in degrees:	6	3	1	
	Combustor Length in m:	0.5	0.5	0.5	
	Fuel Choice:	H_2	H_2	H_2	
	Combustion Equivalence Ratio Φ:	0.45	0.45	0.45	

Table 8.11   Results obtained from TEST V

TEST V					
	CASE	Failure $L = 0.14$	Separation $L_1 = 0.2$		Failure $L = 1$
	Shock Train	100%	74%		21.8%
	Failure Nature	Long Shock Train	-		Thermal Chock at the combustor
Results	Mach Number	Mach Number Profile throughout the Engine for TEST V for L_1=0.14,L_2=0.2, and L_3=1			
	Pressure	Pressure Profile throughout the Engine for TEST V for L_1=0.14,L_2=0.2, and L_3=1			
	Temperature	Temperature Profile throughout the Engine for TEST V for L_1=0.14,L_2=0.2, and L_3=1			

It is apparent that the isolator length affects the self-start of the engine. First, if the isolator is too short, the shock train cannot be contained. Thus, no flow is going to enter the engine due to counter flow. This is shown in the first case. Second, if the length is too long,

thermal choke is bound to happen as shown the third case. This is due the deceleration happening in the isolator. Indeed, the flow as shown is decelerated in the isolator section due to wall friction. Following this intrinsic detail, the flow enters the combustor with a low Mach number that will be slowed down to 1 or lower, causing thermal choke.

In addition to the presented tests, the model could give us an idea on some of the failed configurations could corrected. For instance, increasing the wall temperature of the isolator could delay the shock train failure. For illustration, the first case of TEST III is tested for both $T_w = 300\,K$ and $T_w = 1000\,K$, it was noted that the case with higher temperature is functioning as shown in the plot:

Table 8.12   Results obtained after changing the wall temperature of the failed case in TEST III

Mach Number	
Pressure	

Table 8.12 (continued)

Temperature	

Temperature Profile throughout the Engine for TEST III M_1=3.1 case for M_1=3.1, T_w=300, and T_w=1000
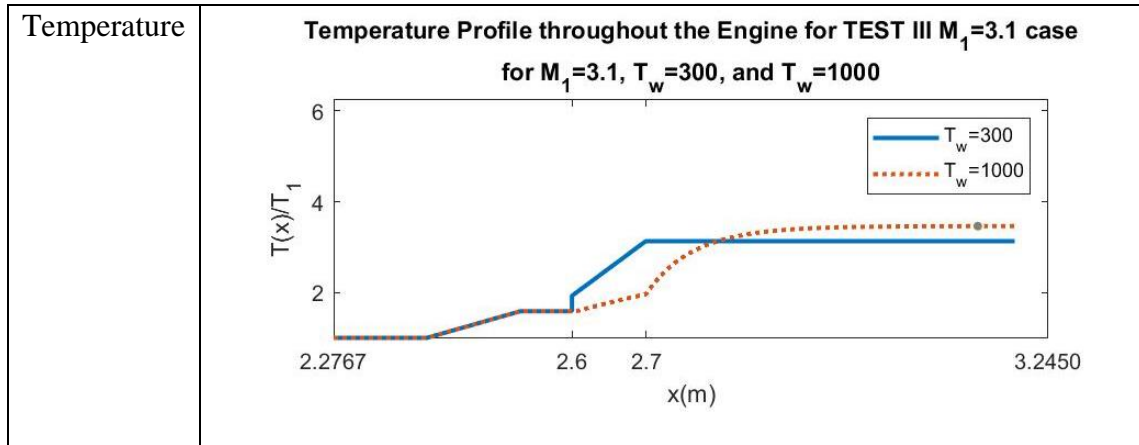
It has been reported that hydrocarbons perform better than hydrogen in lower Mach numbers, as shown in figure 1. Kerosene has been tested for the failure case for TEST III and it showed that the engine can work in this region with a kerosene fuel.

Table 8.13   Results obtained after changing the fuel of the failed case in TEST III

Mach Number	
Pressure	
Temperature	

CHAPTER IX

CONCLUSION

9.1   Insights

Many insights could be drawn from the multiple stages of this work. To name but a few:

- Many parameters contribute in self-start of the scramjet engine. However, the some of the self-start could be summarized on one quantity, M_3 the Mach number at the entry of the combustor. If M_3 is low enough to not produce adequate momentum to counter the pressure, the shock train will travel upstream and stop the inlet from self-starting. Also, if M_3 is low enough to be decelerated to unity, thermal choke conditions will be created in the combustor.

- The altitude, flight Mach number, and ramp angle dictate affect the value of M_3. A small post-shock Mach number will result in a smaller M_3.

- The isolator length also affects the value of the Mach number at the entry of the combustor. A small isolator will result to a higher M_3 compared to a longer one. However, if the isolator is very short, it will not be able to contain the shock train. On the other hand, if the isolator is very long it may lead to thermal choke at the combustor.

- The type of fuel, equivalence ratio, and combustion area expansion angle are responsible for the deceleration of the incoming flow to combustor. Indeed, a smaller area will cause a greater pressure rise given the fact that the pressure is inversely proportional to the area. As the combustion equivalence ratio is approaching unity, the heat release if getting higher thus more flow deceleration. Finally, different fuels have different adiabatic flame temperatures, hence the flow deceleration also differs.

9.2   Future Work

Indeed, the MSU model is still in need of improvements in order to achieve the objectives explained in ?. In the near future, a list of the improvements and features to be implemented is presented below:

- The attached flow within isolator will be updated based on the thermally perfect gas assumption, in particular specific heat will be varied with temperature.

- The effects of the injector geometry and jet area change will be included in the flow calculation of the combustor to achieve better predictions for pressure.

- A decent Nozzle model will be developed to evaluate the thrust and drag of the scramjet engine.

- Parametric study will be extended to demonstrate how the scramjet configuration can be optimized to alleviate engine failure and /or increase thrust.

- The inlet model can be modified to account of internal compression using a reflective shock solver

REFERENCES

[1] *21st International Spaceplane and Hypersonic Systems and Technologies Conference held in XMU*. (2017, March 9). XIAMEN UNIVERSITY. Retrieved June 16, 2022, from https://en.xmu.edu.cn/2017/0308/c10847a267810/page.htm [20]

[2] American Institute of Aeronautics and Astronautics. (1998, January). *Hyper-X Wind Tunnel Program* (NAS 1.15:207317). https://doi.org/10.2514/6.1998-553 [1]

[3] Anderson, G. Exploratory Tests of Two Strut Fuel Injectors for Supersonic Combustion - NASA Technical Reports Server (NTRS). 1 Feb. 1974, ntrs.nasa.gov/citations/19740008383.

[4] Borghi, R. and Murthy, S., 1988. *United States-France Joint Workshop on Turbulent Reactive Flows*. West Lafayette, Ind., USA: School of Mechanical Engineering, Purdue University. [18]

[5] Boyce, R. R., Paull, A., Stalker, R. J., Wendt, M., Chinzei, N., & Miyajima, H., 2000. "Comparison of supersonic combustion between impulse and vitiation-heated facilities". Journal of Propulsion and Power, 16(4), 709-71

[6] Casimir J. Jachimowski. "An analyticaStudy of the Hydrogen-Air Reaction Mechanism With Application to Scramjet Combustion." *NASA*, NASA TechnicaI Paper 2791, National Aeronautics and Space Administration, 1988.

[7] *Des vols hypersoniques pour 2030*. (2018, December 7). Vol En Avion de Chasse. Retrieved June 16, 2022, from https://www.vol-avion-chasse.com/des-vols-hypersoniques-pour-2030/ [2]

[8] Fischer, C., 2014. *Investigation of the Isolator Flow of Scramjet Engines*. PhD. RWTH Aachen University. [15]

[9] Georgiadis, Nicholas, and Michael O'Gara. "Frozen Chemistry Effects on Nozzle Performance Simulations." *38th Fluid Dynamics Conference and Exhibit*, June 2008, https://doi.org/10.2514/6.2008-3969.

[10] Gopal, V., 2015. *REDUCED-ORDER ANALYSIS OF DUAL MODE SUPERSONIC COMBUSTION RAMJET PROPULSION SYSTEM*. Master of Science. University of Texas at Arlington. [9]

[11] History of Ramjet and Scramjet Propulsion Development for U.S. Navy Missiles. (1997b). *JOHNS HOPKINS APL TECHNICAL DIGEST*, *18*(2), 234–243. [3]

[12] *Les avions hypersoniques*. (2022, January 18). Vol En Avion de Chasse. Retrieved June 16, 2022, from https://www.vol-avion-chasse.com/les-avions-hypersoniques/ [4]

[13] Lisa Bouheraoua. Simulation aux grandes échelles et modélisation de la combustion supersonique. Mécanique des fluides [physics.class-ph]. INSA de Rouen, 2014. Français. ffNNT : 2014ISAM0022ff. fftel-01197487f [8]

[14] Lytle, John. Numerical Propulsion System Simulation (NPSS) 1999 Industry Review - NASA Technical Reports Server (NTRS). 1 Aug. 2000, ntrs.nasa.gov/citations/20000120213.

[15] Mcbride, Bonnie. Coefficients for Calculating Thermodynamic and Transport Properties of Individual Species - NASA Technical Reports Server (NTRS). 1 Oct. 1993, ntrs.nasa.gov/citations/19940013151.

[16] McClinton, C.R. (2008) High Speed/Hypersonic Aircraft Propulsion Technology Development. In Advances on Propulsion Technology for High-Speed Aircraft (pp. 1-1 – 1-32). Educational Notes RTO-EN-AVT-150, Paper 1. Neuilly-sur-Seine, France: RTO. Available from: http://www.rto.nato.int. [19]

[17] Murthy, S. and Curran, E., 2001. *Scramjet Propulsion*. Reston, VA: American Institute of Aeronautics and Astronautics. [17]

[18] Ortwerth, P. J., "Scramjet Vehicle Integration," American Institute of Aeronautics and Astronautics, Washington DC, 2001. [5]

[19] ROBERTS, K., 2008. *ANALYSIS AND DESIGN OF A HYPERSONIC SCRAMJET ENGINE WITH A STARTING MACH NUMBER OF 4.0*. Master of Science. University of Texas at Arlington. [13]

[20] Segal, C., 2009. *The Scramjet Engine PROCESSES AND CHARACTERISTICS*. New York: Cambridge University Press. [16]

[21] Smart, Michael K., "Scramjets," Centre for Hypersonics, The University of Queensland, Brisbane, Australia, 2008. [6]

[22] Svensson, G., 2020. *1D Scramjet Model*. Master of Science. MASSACHUSETTS INSTITUTE OF TECHNOLOGY.[11]

[23] The Math Works, Inc. *MATLAB*. Version 2019a, The Math Works, Inc., 2020. Computer Software. [21]

[24] Thompson, E., Henry, K., & Williams, L. (2005, June 20). *Faster Than a Speeding Bullet: Guinness Recognizes NASA Scramjet*. NASA. Retrieved June 16, 2022, from https://www.nasa.gov/home/hqnews/2005/jun/HQ_05_156_X43A_Guinness.html [7]

[25] Tran, K., 2010. *One Dimensional Analysis Program for Scramjet and Ramjet Flowpaths*. Master of Science. Virginia Polytechnic Institute and State University. [10]

[26] TU, Q., 2013. *EFFECTS OF FUEL INJECTION ON MIXING AND UPSTREAM INTERACTIONS IN SUPERSONIC FLOW*. PhD. University of Florida. [14]

[27] *U.S. Standard Atmosphere Vs. Altitude*. www.engineeringtoolbox.com/standard-atmosphere-d_604.html. Accessed 26 Oct. 2022.

[28] VU, L., 2018. *QUASI-ONE-DIMENSIONAL SCRAMJET COMBUSTOR FLOW SOLVER USING THE NUMERICAL PROPULSION SYSTEM SIMULATION*. Master of Science. University of Texas at Arlington. [12]

APPENDIX A

MSU MODEL CODE

A.1　Main code

```
clear

clc

close all


%% Input Document:

Choke=0;

%% Inlet:

% Free Stream Conditions:

M1=3.1;%input('Enter free stream mach number: ');

h=20000;%input('Enter altitude in meters between -1000m to 80000m: ');

% Inlet Design:

D1=1;%input('Enter the inlet entry diameter in meters: ');

theta=20;%input('Enter the ramp angle in degrees 0°< ? <90°: ');

a2D=2;%input('Enter the aspect ratio: ');

RorE=1; %1 corresponds to rectangular cross section, 0 to Elliptic

% output:

ALLin=inlett(h,M1,D1,a2D,theta,RorE);


% Inlet entry Flow Characteristics:

P1=ALLin(2,1);

T1=ALLin(3,1);

rho1=ALLin(4,1);
```

```matlab
%Inlet Exit Flow Characteristics:

M2=ALLin(1,2);

P2=ALLin(2,2);

T2=ALLin(3,2);

rho2=ALLin(4,2);


% Other parameters:

mdota=ALLin(5,1);

Pstar=ALLin(5,2);

Xin=ALLin(6,1);

xavg=ALLin(6,2);

D2=ALLin(7,1);

w2=ALLin(7,2);

A2=ALLin(8,1);

nKE=ALLin(8,2);


%Post processing:
% Points
Nptsi1=20;

Nptsi2=5;

xi1= 0:xavg/Nptsi1:xavg;

xi2= xavg:(Xin-xavg)/Nptsi2:Xin;
```

```matlab
xi=[xi1 xi2];

%xf= [x3 x3+x2];

Pi=zeros(1,length(xi));

Pi(1:length(xi1))=P1;

Pi(length(xi1):end)=P2;

Mi=zeros(1,length(xi));

Mi(1:length(xi1))=M1;

Mi(length(xi1):end)=M2;

Ti=zeros(1,length(xi));

Ti(1:length(xi1))=T1;

Ti(length(xi1):end)=T2;

rhoi=zeros(1,length(xi));

rhoi(1:length(xi1))=rho1;

rhoi(length(xi1):end)=rho2;


Plotin=0;
if Plotin==1
    figure
    subplot(2,2,1);
    plot(xi,Mi, 'linewidth', 2)
    ylim([min(Mi) max(Mi)])
    title("Mach number profile")
    ylabel("M",'FontSize',10)
```

```matlab
    subplot(2,2,2);

    plot(xi,Pi, 'linewidth', 2)

    ylim([min(Pi) max(Pi)])

    title("Pressure profile")

    ylabel("P in (Pa)",'FontSize',10)


    subplot(2,2,3);

    plot(xi,Ti, 'linewidth', 2)

    ylim([min(Ti) max(Ti)])

    title("Temperature profile")

    ylabel("T in (K)",'FontSize',10)


    subplot(2,2,4);

    plot(xi,rhoi, 'linewidth', 2)

    ylim([min(rhoi) max(rhoi)])

    title("Density profile")

    ylabel("\rho in kg/m^3",'FontSize',10)


    sgtitle('Flow characteristic in the inlet')
end


%Inlet results:
```

```matlab
INLET=[xi' Mi' Pi' Ti' rhoi'];

%% Saving Results:

yes_noIN=0;

if yes_noIN==1

    titles=["x" "M" "P" "T" "rho"];

    inlet=[titles ;xi' Mi' Pi' Ti' rhoi'];

    writematrix(inlet,'inlet.csv')

end


%% Isolator:

%% Geometry:

x2=0;

xd=0.1;

D=D2;

w=w2;

%A2=w*D;


%% Isolator Chamber set-up:




%% Thermodynamic properties
```

%specific Heat

% Air composition:

Xair=[.21*0.032 .79*0.028]./((.21*0.032)+(.79*0.028));

MWair=Xair(1)*0.032+Xair(2)*0.028;

Yair=[Xair(1)*0.032 Xair(2)*0.028]./MWair;

cp=(Yair(1)*spec_Cp(entry_species('O2'),

T2)/0.032)+(Yair(2)*spec_Cp(entry_species('N2'), T2)/0.028);

R=8.314/MWair;%287;

gamma=cp/(cp-R);%cp/cv;

Tw=300; %wall temperature in K

%Friction Coefficient

%Cf=.01;%.02296/((rho2*M2*sqrt(gamma*T2*R)*(xd-x2)/(3.12*1e-

5))^.139);%1*.01;%;

ALLis=isolATT(M2,P2,T2,rho2,A2,D,xd,Tw,R,gamma,RorE);%x M P T rho

ISLOTAR=ALLis;

   sIS=size(ALLis);

      for i=1:sIS(1)

        if ALLis(i,2)<=1

          Choke=1;

          fprintf('FAILURE AT THE ISOLATOR DUE TO THERMAL CHOKE\n')

```
            break

        end

    end

if Choke==0


PlotisATT=1;

if PlotisATT==1

    figure

    plot(ALLis(:,1),ALLis(:,2), 'linewidth', 1.5); hold on;

    plot(ALLis(:,1),ALLis(:,3)/P2, 'linewidth', 1.5); hold on;

    plot(ALLis(:,1),ALLis(:,4)/T2, 'linewidth', 1.5); hold on;

    plot(ALLis(:,1),ALLis(:,5)/rho2, 'linewidth', 1.5);

    legend("M(x)","P(x)/P2","T(x)/T2","\rho (x)/\rho_2");

    title("Isolator with no separation")

end

yes_noIS=0;

if yes_noIS==1

    titles=["x" "M" "P" "T" "rho"];

    isolatorATT=[titles ;ALLis(:,1) ALLis(:,2) ALLis(:,3) ALLis(:,4) ALLis(:,4)];

    writematrix(isolatorATT,'isolator.csv')

end

%% Combustor with no separation:

% Updated Gas properties from the isolator:
```

```matlab
        cp=(Yair(1)*spec_Cp(entry_species('O2'),

ALLis(end,4))/0.032)+(Yair(2)*spec_Cp(entry_species('N2'), ALLis(end,4))/0.028);

        gamma1=cp/(cp-R);

        % Fuel choice and combustion properties:

        N=5;    %number of species

        %speName = {'H2', 'O2', 'H2O', 'N2'};

        speName = {'C2H4', 'O2', 'H2O','CO2','N2'};

        %speMW   = [0.002, 0.032, 0.018, 0.028];

        speMW   = [0.028, 0.032, 0.018, .044, 0.028];

        %v = [-1 -0.5 1 0];  %st. coefficient

        v = [-1 -3 2 2 0];

        %vr = [1 0.5 0 .5*79/21];    %reactant coefficient:

        vr = [1 3 0 0 3*79/21];

        FAu=0.1;    %Global Equivalence Ratio:


        %Combustion chamber geometry

        x4=.5;

        deg=3;  %Geometry expansion angle in degrees

        %Calculation

        ALLcATT=combATT(ALLis,gamma1,R,x4,A2,D,deg,N,speName,speMW,v,vr,FAu); %

x M P T rho Pst/Pst3 Tst/Tst3 A/A3

        COMBUSTOR=ALLcATT;

          sIS=size(ALLcATT);
```

```matlab
    for i=1:sIS(1)

        if ALLcATT(i,2)<=1

            Choke=1;

            fprintf('FAILURE AT THE COMBUSTOR DUE TO THERMAL CHOKE\n')

            break

        end

    end

ALLcATT(:,2);

if Choke==0


%Plot resuts:

PlotisATT=1;

if PlotisATT==1

    figure

    plot(ALLcATT(:,1),ALLcATT(:,2), 'linewidth', 1.5); hold on;

    plot(ALLcATT(:,1),ALLcATT(:,3)/ALLis(end,3), 'linewidth', 2); hold on;

    plot(ALLcATT(:,1),ALLcATT(:,4)/ALLis(end,4), 'linewidth', 1.5); hold on;

    plot(ALLcATT(:,1),ALLcATT(:,5)/ALLis(end,5), 'linewidth', 1.5);

    plot(ALLcATT(:,1),ALLcATT(:,end), 'linewidth', 1.5);

    legend("M(x)","P(x)/P_3","T(x)/T_3","\rho (x)/\rho_3","A(x)/A_3");

    title("Combustor with no separation")

end
```

```matlab
%% Separation existance check:

Pcmax=max(ALLcATT(:,3));


if Pcmax<Pstar

index_cmax=find(ALLcATT(:,3)==Pcmax);

Mcmax=ALLcATT(index_cmax,2);

if (Mcmax/ALLis(end,2))<.762

%% Isolator with separation:

    ALLsep=isolSEP(M2,P2,T2,rho2,R,gamma,cp,A2,D,Pcmax,Tw,xd,ALLis,RorE);

    ISLOTAR=ALLsep;

    if ALLsep(:,2)==0 %ALLsep==0%

        ALLsep(:,4)=((max(ALLcATT(:,4))-ALLsep(1,4))*(ALLsep(:,1)-

ALLsep(1,1))/(ALLsep(end,1)-ALLsep(1,1)))+ALLsep(1,4);

        ISLOTAR=ALLsep;

        ALLcATT(:,2)=0;

        ALLcATT(:,3)=ALLsep(1,3);

        ALLcATT(:,4)=max(ALLcATT(:,4));

        ALLcATT(:,5)=ALLsep(1,5);

        COMBUSTOR=ALLcATT;

        fprintf('FAILURE AT THE ISOLATOR DUE TO LONG SHOCK TRAIN\n')

    else

    sIS=size(ALLsep);

        for i=1:sIS(1)
```

```matlab
        if ALLsep(i,2)<=1

            Choke=1;

            fprintf('FAILURE AT THE ISOLATOR DUE TO THERMAL CHOKE')

            break

        end

    end

    if Choke==0


    PlotisSEP=1;

    if PlotisSEP==1

        figure

        plot(ALLsep(:,1),ALLsep(:,2), 'linewidth', 1.5); hold on;

        plot(ALLsep(:,1),ALLsep(:,3)/P2, 'linewidth', 1.5); hold on;

        plot(ALLsep(:,1),ALLsep(:,4)/T2, 'linewidth', 1.5); hold on;

        plot(ALLsep(:,1),ALLsep(:,5)/rho2, 'linewidth', 1.5);

        legend("M(x)","P(x)/P2","T(x)/T2","\rho (x)/\rho_2");

        title("Isolator with separation")

    end


    %% Combustor with separation:

    % Updated Gas properties from the isolator:

    cp=(Yair(1)*spec_Cp(entry_species('O2'),

ALLsep(end,4))/0.032)+(Yair(2)*spec_Cp(entry_species('N2'), ALLsep(end,4))/0.028);
```

```matlab
gamma2=cp/(cp-R);


ALLcSEP=combSEP(ALLcATT,ALLsep,Pcmax,index_cmax,gamma2,R,x4,A2,D,deg,N,speNa
me,speMW,v,vr,FAu);
        COMBUSTOR=ALLcSEP;

        sIS=size(ALLcATT);

        for i=1:sIS(1)

          if ALLcSEP(i,2)<=1

            Choke=1;

            fprintf('FAILURE AT THE COMBUSTOR DUE TO THERMAL CHOKE')

            break

          end

        end

    if Choke==0


      %Plot resuts:

      PlotisSEP=1;

      if PlotisSEP==1

        figure

        plot(ALLcSEP(:,1),ALLcSEP(:,2), 'linewidth', 1.5); hold on;

        plot(ALLcSEP(:,1),ALLcSEP(:,3)/ALLsep(end,3), 'linewidth', 1.5); hold on;

        plot(ALLcSEP(:,1),ALLcSEP(:,4)/ALLsep(end,4), 'linewidth', 1.5); hold on;

        plot(ALLcSEP(:,1),ALLcSEP(:,5)/ALLsep(end,5), 'linewidth', 1.5); hold on;
```

```matlab
        plot(ALLcSEP(:,1),ALLcSEP(:,end), 'linewidth', 1.5);

        legend("M(x)","P(x)/P_3","T(x)/T_3","\rho (x)/\rho_3","A(x)/A_3");

        title("Combustor with separation")

    end

end

    end

    end

end




%% Failure:

else

    fprintf('FAILURE AT THE COMBUSTOR: VERY HIGH PRESSURE\n')

end

end

%% Nozzle

%% Overall Profile:

x=[xi'; Xin+ISLOTAR(:,1); Xin+xd+COMBUSTOR(:,1)];

%Mach:

figure

yyaxis left

plot(x,[INLET(:,2);ISLOTAR(:,2);COMBUSTOR(:,2)], 'LineWidth',2); hold on
```

```matlab
        plot(x,[INLET(:,4)/T1;ISLOTAR(:,4)/T1;COMBUSTOR(:,4)/T1],':k', 'LineWidth',2);

hold on

        plot(x,[INLET(:,5)/rho1;ISLOTAR(:,5)/rho1;COMBUSTOR(:,5)/rho1],'--g',

'LineWidth',2)

        xlabel("x(m)")

        ylabel("M(x), T(x)/T_1, \rho(x)/\rho_1")

        xlim([x(1) x(end)])

        xticks([x(1):.5:x(end) x(end)])

        pbaspect([2 1 1])

        yyaxis right

        plot(x,[INLET(:,3)/P1;ISLOTAR(:,3)/P1;COMBUSTOR(:,3)/P1],'-.', 'LineWidth',2)

        xlim([x(1) x(end)])

        ylabel("P(x)/P_1")

        legend("M(x)","T(x)/T_1","\rho (x)/\rho_1", "P(x)/P_1")

        title("Mach number, Pressure Profile, Temperature Profile, and Density Profile

throughout the Engine")

        pbaspect([2 1 1])

        xticks([x(1):.5:x(end) x(end)])


        yes_no=1;

        Mach=[INLET(:,2);ISLOTAR(:,2);COMBUSTOR(:,2)];

        Pressure=[INLET(:,3);ISLOTAR(:,3);COMBUSTOR(:,3)];

        Temperature=[INLET(:,4);ISLOTAR(:,4);COMBUSTOR(:,4)];
```

```
Density=[INLET(:,5);ISLOTAR(:,5);COMBUSTOR(:,5)];

if yes_no==1

    titles=["x" "M" "P" "T" "rho"];

    SCRAM=[titles ;x Mach Pressure Temperature Density];

    writematrix(SCRAM,'FLOWCASEIII1ss.csv')

end


end
```

A.2   Inlet

A.2.1   USAAP

```
clc

close all

clear

% U.S. Standard Atmosphere Air Properties - SI Units


%% Altitude: in meters

h1=-1000:1000:10000;

h2=15000:5000:30000;

h3=40000:10000:80000;

% Altitude column:

h=[h1'; h2'; h3'];


%% Temperature: in Celsius
```

T1=[21.5 15 8.5 2 -4.49 -10.98 -17.47 -23.96 -30.45 -36.94 -43.42 -49.9];

T2=[-56.5 -56.5 -51.6 -46.64 -22.8 -2.5 -26.13 -53.57 -74.51];

% Temperature column:

T=[T1'; T2'];

%% Gravity: in m/s^2

g1=[9.81 9.807 9.804 9.801 9.797 9.794 9.791 9.788 9.785 9.782 9.779 9.776];

g2=[9.761 9.745 9.730 9.715 9.684 9.654 9.624 9.594 9.564];

% Gravity column:

g=[g1'; g2'];

%% Absolute Pressure: x10^4 Pa

P1=[11.39 10.13 8.988 7.95 7.012 6.166 5.405 4.722 4.111 3.565 3.080];

P2=[2.65 1.211 0.5529 0.2549 0.1197 0.0287 0.007978 0.002196 0.00052 0.00011];

% Pressure column:

P=[P1'; P2'];

%% Density: in kg/m^3

rho1=[1.347 1.225 1.112 1.007 0.9093 0.8194 0.7364 0.6601 0.59 0.5258];

rho2=[0.4671 0.4135 0.1948 0.08891 0.04008 0.01841 0.003996 0.001027];

rho3=[0.0003097 0.00008283 0.00001846];

% Density column:

rho=[rho1'; rho2'; rho3'];

%% Dynamic Viscocity: in x10^-5 N s/m^2

mu1=[1.821 1.789 1.758 1.726 1.694 1.661 1.628 1.595 1.561 1.527 1.493 1.458];

mu2=[1.422 1.422 1.448 1.475 1.601 1.704 1.584 1.438 1.321];

mu=[mu1'; mu2'];

titles=["h in m" "T in °C" "g in m/s^2" "P x10^4 Pa" "Density in kg/m^3" "Dynamic Viscocity in x10^-5 N s/m^2"];

test=[h T g P rho mu];

Atmosphere=[titles ;h T g P rho mu];

%% Exporting as .cvs File

writematrix(Atmosphere,'Atmosphere.csv')

A.2.2   Interpolation

```
function properties=USAAP(h, TABLE)

H=h;

A=TABLE;


[numrows, numcols]=size(A);


for i=1:numrows

  if H<A(1,1)

    properties=A(1,:);
```

```matlab
        break

    elseif H>A(end,1)

        properties=A(end,:);

        break

    else

        if H==A(i,1)

            properties=A(i,:);

            break

        elseif H<A(i,1)

            properties=A(i-1,:)+(A(i+1,:)-A(i-1,:))*(H-A(i-1,1))/(A(i+1,1)-A(i-1,1));

            break

        end

    end

end

end
```

A.2.3   Main code

```matlab
function ALLin1=inlett(h,M1,D1,a2D,theta,RorE)

%% Importing data:

Atmosphere1=readtable('Atmosphere.csv');

Atmosphere=Atmosphere1.Variables;

%% Free Stream conditions


% other parameters from table:
```

```matlab
properties=USAAP(h, Atmosphere);

T1=properties(2)+273.15; %Temperture in K

P1=properties(4)*10^4; %Pressure in Pa

rho1=properties(5); % Density in kg/m^3

R=P1/rho1/T1;   %Gas constant

% Air composition:

Xair=[.21*0.032 .79*0.028]./((.21*0.032)+(.79*0.028));

MWair=Xair(1)*0.032+Xair(2)*0.028;

Yair=[Xair(1)*0.032 Xair(2)*0.028]./MWair;

cp=(Yair(1)*spec_Cp(entry_species('O2'),
T1)/0.032)+(Yair(2)*spec_Cp(entry_species('N2'), T1)/0.028);

gamma=cp/(cp-R);




%% SHOCK WAVES
%%%%%%%%%%%%%%%%%%%%%%%%%%%%%%%%%%%%%%%%%%%
%%%
beta=theta2beta(gamma,M1,theta); %in degrees
%calculations:
rho2=rho1*(gamma+1)*((M1*sind(beta))^2)/(2+((gamma-1)*((M1*sind(beta))^2)));
P2=P1*(1+gamma*((M1*sind(beta))^2)*(1-rho1/rho2));
T2=T1*(1+(gamma-1)*((M1*sind(beta))^2)*(1-(rho1/rho2)^2)/2);
```

```
M2=((T1*(1+(M1^2)*(gamma-1)/2)/T2-1)*2/(gamma-1))^.5;
```

```
%% State Summary

header1=["" "Free stream" "Inlet exit"];

header2=["Mach number";"Pressure";"Temperature";"Density"];

state=[M1 M2; P1 P2; T1 T2; rho1 rho2];

State=[header1; header2 state];

disp(State)

%kinetic efficiency:

nKE=1-(2*(P1/P2)^(gamma-(1/gamma))/(gamma-1)/(M1^2));
```

```
%% Properties at the sonic state:

Tst1=T1*(1+((gamma-1)*(M1^2)/2));

Tstar=Tst1/(gamma-1)/2;

rhost1=rho1*(Tst1/T1)^(1/(gamma-1));

rhostar=rhost1/(((gamma+1)/2)^(1/(gamma-1)));

Pst1=P1*(Tst1/T1)^(gamma/(gamma-1));

Pstar=Pst1/(((gamma+1)/2)^(gamma/(gamma-1)));
```

```
%% Inlet Length:

CR=(((1+(gamma-1)*(M1^2)/2)*2/(gamma-1))^(0.5*(gamma+1)/(gamma-1)))/M1;

if RorE==0

    A1=pi*D1*D1*a2D;
```

```matlab
    A2=A1*rhostar*sqrt(Tstar/T2)/M2/rho2/CR;

    polynomial=[1 -2*D1 (D1^2)-(A2*4/a2D/pi)];

    d=(roots(polynomial));

    d=d(d<D1);

    X=d/tand(theta);

    D2=D1-d;

    w2=pi*a2D*D2;

elseif RorE==1

    A1=D1*D1*a2D;

    A2=A1*rhostar*sqrt(Tstar/T2)/M2/rho2/CR;

    polynomial=[1 -2*D1 (D1^2)-(A2/a2D)];

    d=(roots(polynomial));

    d=d(d<D1);

    X=d/tand(theta);

    D2=D1-d;

    w2=a2D*D2;

end



%% Mass Flow Rate:

R2=P2/rho2/T2;

mdot=rho2*A2*M2*(gamma*R2*T2)^.5;
```

%% Display the inlet design parameters:

fprintf('The area of the inlet exit/throat is %d m^{2}\n', A2)

fprintf('The length of the inlet is %f m\n', X)

fprintf('The maximum mass flow rate allowed for Ma= %f is %f kg/s\n', M1, mdot)

fprintf('The mass flow rate is %f kg/s\n', mdot)

fprintf('P^* is %f\n',Pstar)

fprintf('The kinetic efficiency for this inlet is %f\n', nKE)

%%

%% Plotting the results:

% The average location of the jump:

xavg=X-(X*(D1-d)/2/D1);

ALLin1=[state; mdot Pstar; X xavg; D2 w2; A2 nKE];

end

A.2.4   Find β

function BETA=theta2beta(Gamma,Mach,Theta)

gamma=Gamma;

M1=Mach;

theta=Theta;

```matlab
        f=@(beta) (2.*cotd(beta).*(((M1.*sind(beta)).^2)-

1)./(2+(gamma+cosd(2*beta)).*(M1^2)));


        deri_f1=@(beta) (4*(M1^2).*cotd(beta).*sind(2*beta).*(((M1.*sind(beta)).^2)-

1)./((2+(gamma+cosd(2.*beta)).*(M1^2))^2));

        deri_f2=@(beta) (2.*((cotd(beta)^2+1).*(((M1.*sind(beta)).^2)-

1)./(2+(gamma+cosd(2.*beta)).*(M1^2))));

        deri_f3=@(beta)

(4.*cotd(beta).*cosd(beta).*sind(beta).*(M1^2)./(2+(gamma+cosd(2.*beta)).*(M1^2)));


        %% Newton Raphson Method
        beta0=((gamma+1)/2)*theta*pi/180;
        y=f(beta0)-tand(theta);
        deri_y=deri_f1(beta0)-deri_f2(beta0)+deri_f3(beta0);
        Beta=beta0-y/deri_y;
        while abs(Beta-beta0)>1e-05
            %Our function:
            beta0=Beta;
            y=f(beta0)-tand(theta);
            deri_y=deri_f1(beta0)-deri_f2(beta0)+deri_f3(beta0);

            Beta=beta0-y/deri_y;
        end
```

112

BETA=Beta;

End

A.3   Isolator

A.3.1   Isolator attached flow

```
function ALLis1=isolATT(M2,P2,T2,rho2,A2,D,xd,Tw,R,gamma,RorE)


%% Geometry

x2=0;

dx=.001;

xis=x2:dx:xd;

if RorE==1

   w=A2/D;

   pe2=(w+D)*2;

elseif RorE==0

   pe2=pi*(3*(w+D)/2-sqrt((3*w+D)*(w+3*D)/4)); %Ramanujan apprximation

end

DH=4*A2/pe2;


Tst2=T2*(1+((gamma-1)*(M2^2)/2));

Pst2=P2*((Tst2/T2)^(gamma/(gamma-1)));
```

```matlab
Pr=.715;%(2.45*1e-5)*cp/(180*1e-03);

Tstar=.5*T2+.5*Tw+(.16*(Pr^(1/3))*(gamma-1)*T2*(M2^2)/2);

rhostar=rho2*T2/Tstar;

mustar=1.722*(1e-5)*((Tstar/273.15)^(3/2))*(273.15+111)/(Tstar+111);

Cf=.02296/((rhostar*M2*sqrt(gamma*T2*R)*(xd-x2)/mustar)^.139)/2;


ALLis1=isola(xis); %x M P T rho
sIS=size(ALLis1);
    for i=1:sIS(1)
       if ALLis1(i,2)<=1
           figure
           plot(ALLis1(:,1),ALLis1(:,2), 'linewidth', 1.5); hold on;
           plot(ALLis1(:,1),ALLis1(:,3)/P2, 'linewidth', 1.5); hold on;
           plot(ALLis1(:,1),ALLis1(:,4)/T2, 'linewidth', 1.5); hold on;
           plot(ALLis1(:,1),ALLis1(:,5)/rho2, 'linewidth', 1.5);
           legend("M(x)","P(x)/P2","T(x)/T2","\rho (x)/\rho_2");
           title("Thermal Choke at the Isolator")
           break
       end
    end
function isolator=isola(xis)
%{
global M2
```

```matlab
global gamma

global A2

global D

global DH

global isoL

global T2

global P2

global rho2

global R

global pe2

global Cf

global Tst2

global Pst2

global x2

global xd

global dx

%}



%% Isolator parameters:


%stagnation properties:

x=xis;
```

```matlab
% Initializing

Pt= zeros(1,length(xis));

MM2= zeros(1,length(xis));

rho= zeros(1,length(xis));

P= zeros(1,length(xis));




Pt(1)=Pst2;

rho(1)=rho2;

P(1)=P2;

T(1)=T2;

MM2(1)=M2;


dM2dx = @(x,MM2) (MM2)*gamma*2*Cf*(MM2^2)*(1+((gamma-
1)*(MM2^2)/2))/(1-(MM2^2))/DH;

    for i=1:(length(x)-1)

      % calculation loop

      k_1 = dM2dx(x(i),MM2(i));

      k_2 = dM2dx(x(i)+0.5*dx,MM2(i)+0.5*dx*k_1);

      k_3 = dM2dx((x(i)+0.5*dx),(MM2(i)+0.5*dx*k_2));

      k_4 = dM2dx((x(i)+dx),(MM2(i)+k_3*dx));

      MM2(i+1) = MM2(i) + dx*(k_1+2*k_2+2*k_3+k_4)/6;  % main equation
```

```matlab
end


for i=1:(length(xis)-1)

    T(i+1) = Tst2/(1+((gamma-1)*(MM2(i+1)^2)/2));

end

%{

for i=1:(length(x)-1)  % calculation loop

    dPtdx = @(x,Pt) -Pt*2*gamma*(MM2(i)^2)*Cf/DH;


    k_1 = dPtdx(x(i),Pt(i));

    k_2 = dPtdx(x(i)+0.5*dx,Pt(i)+0.5*dx*k_1);

    k_3 = dPtdx((x(i)+0.5*dx),(Pt(i)+0.5*dx*k_2));

    k_4 = dPtdx((x(i)+dx),(Pt(i)+k_3*dx));

    Pt(i+1) = Pt(i) + (dx*(k_1+2*k_2+2*k_3+k_4)/6);  % main equation


end

for i=1:(length(x)-1)  % calculation loop

    P(i+1) = Pt(i+1)/((Tst2/T(i+1))^(gamma/(gamma-1)));  % main equation


end
```

```matlab
%}
    for i=1:(length(x)-1)  % calculation loop

        dPdx = @(x,P) P*2*gamma*(MM2(i)^2)*Cf*(1-((gamma-1)*(MM2(i)^2))-2)/DH/(1-
MM2(i)^2);


        k_1 = dPdx(x(i),P(i));

        k_2 = dPdx(x(i)+0.5*dx,P(i)+0.5*dx*k_1);

        k_3 = dPdx((x(i)+0.5*dx),(P(i)+0.5*dx*k_2));

        k_4 = dPdx((x(i)+dx),(P(i)+k_3*dx));

        P(i+1) = P(i) + (dx*(k_1+2*k_2+2*k_3+k_4)/6);  % main equation


    end


    for i=1:(length(xis)-1)

        rho(i+1) = P(i+1)/T(i+1)/R;  % main equation

    end


    isolator=[xis' MM2' P' T' rho'];%Pt'


    end


end
```

A.3.2 Isolator Detached flow

```
function ALLsep1=isolSEP(M2,P2,T2,rho2,R,gamma,cp,A2,D,Ps,Tw,xd,ALLis,RorE)

%% Geometry

x2=0;

dx=.001;

xis=x2:dx:xd;

if RorE==1

    w=A2/D;

    pe2=(w+D)*2;

elseif RorE==0

    pe2=pi*(3*(w+D)/2-sqrt((3*w+D)*(w+3*D)/4)); %Ramanujan apprximation

end

DH=4*A2/pe2;


Pr=.715;%(2.45*1e-5)*cp/(180*1e-03);

Tstar=.5*T2+.5*Tw+(.16*(Pr^(1/3))*(gamma-1)*T2*(M2^2)/2);

rhostar=rho2*T2/Tstar;

mustar=1.722*(1e-5)*((Tstar/273.15)^(3/2))*(273.15+111)/(Tstar+111);

Cf=.02296/((rhostar*M2*sqrt(gamma*T2*R)*(xd-x2)/mustar)^.139)/2;


%calculations parameters:

Tst2=T2*(1+((gamma-1)*(M2^2)/2));

%Pst2=P2*((Tst2/T2)^(gamma/(gamma-1)));
```

119

```matlab
pri=Ps/P2;

mdot=rho2*A2*M2*sqrt(gamma*T2*R);

g2=mdot*sqrt((gamma-1)*cp*Tst2)/P2/A2;

f2=(P2*A2+mdot*M2*sqrt(gamma*R*T2))/P2/A2;


%% Shock-train correlation
isoL=((gamma-1)*log(pri)/gamma/2)+(((((pri-1)/(f2-pri)/(f2-1))+(log(pri*(f2-1)/(f2-
pri))/f2))*(g2^2)/gamma/f2/44.5/Cf);

isoL=DH*isoL;

if isoL<0

    isoL=xd;

elseif isoL>xd

    fprintf('LONG SHOCK TRAIN LENGTH Initial Estimation %f \n', isoL)

    %ALLsep1=0;

    isoL=xd;

end


%if isoL>0 && isoL<=xd

if isoL>0 && isoL<=xd

Pis=zeros(1,length(xis));

for i=1:length(xis)

    Pis(i)=ALLis(i,3);

    if ((xd-xis(i))-isoL)<=0
```

```
            index=i;

             break

          end

      end


      ytry=[];


      for i=0:length(xis)-index-1


          [xx,y]=ode113(@my_ode1, [xis(index+i) xd], [(ALLis(index+i,2)^2) 1
ALLis(index+i,3)]);%log(isolator(index+27,3))
          ytry=[ytry abs((y(end,3)/P2)-(Ps/P2))];


      end

      iu=find(ytry==min(ytry));

      [xx,y]=ode113(@my_ode1, [xis(index+iu) xd], [(ALLis(index+iu,2)^2) 1
ALLis(index+iu,3)]);

      Tst2=ALLis(index+iu,4)*(1+((gamma-1)*(ALLis(index+iu,2)^2)/2));

      Tsep=Tst2./(1+((gamma-1)*y(:,1)/2));

      rhosep=y(:,3)./Tsep/R;

      yy=[xx sqrt(y(:,1)) y(:,3) Tsep rhosep y(:,2)];%xx M P T rho Ac/A

      size(yy)
```

```matlab
    size([xis(1:index+iu)' ALLis(1:index+iu,2) ALLis(1:index+iu,3) ALLis(1:index+iu,4)

ALLis(1:index+iu,5) ones(index+iu,1)])

    Aissep=[xis(1:index+iu)' ALLis(1:index+iu,2) ALLis(1:index+iu,3) ALLis(1:index+iu,4)

ALLis(1:index+iu,5) ones(index+iu,1)];

    ALLsep1=[Aissep;yy];

    sIS=size(ALLsep1);

        for i=1:sIS(1)

            if ALLsep1(i,2)<=1

                figure

                plot(ALLsep1(:,1),ALLsep1(:,2), 'linewidth', 1.5); hold on;

                plot(ALLsep1(:,1),ALLsep1(:,3)/P2, 'linewidth', 1.5); hold on;

                plot(ALLsep1(:,1),ALLsep1(:,4)/T2, 'linewidth', 1.5); hold on;

                plot(ALLsep1(:,1),ALLsep1(:,5)/rho2, 'linewidth', 1.5);

                legend("M(x)","P(x)/P2","T(x)/T2","\rho (x)/\rho_2");

                title("Thermal Choke at the Isolator Due to Separation")

                break

            end

        end

    if (xis(iu+index))<=.001

        ALLsep1(:,2)=0;

        ALLsep1(:,3)=Ps;

        ALLsep1(:,4)=ALLsep1(end,4);

        ALLsep1(:,5)=ALLsep1(end,5);
```

```matlab
    %ALLsep1=0;

    end


    fprintf('SHOCK TRAIN LENGTH %f m \n', xd-xis(iu+index))

    end


    function dy=my_ode1(~,y)
    %{
    global M2
    global Cf
    global gamma
    global A2
    global AcA2
    global DH
    %}



    dy3=y(3)*89*Cf*y(1)*gamma/DH/2;%sqrt(pi/4/A2)/2;
    dy1=-y(1)*(1+(gamma-
1)*y(1)/2)*((dy3*2/gamma/y(1)/y(3))+(4*Cf*y(1)*gamma/DH))/y(2);%93*Cf*((pi/A2/4)^.5)/y(
2);
    dy2=(dy3*(1-y(1)*(1-gamma*(1-y(2)))))/gamma/y(1)/y(3))+(4*Cf*(1+(gamma-
1)*y(1))/2/DH);
```

%dy2=89*Cf*((pi/A2/4)^.5)*(1-y(1)*(1-gamma*(1-

y(2))))/2+(4*Cf*((pi/A2/4)^.5)*(1+(gamma-1)*y(1))/2);

dy=y;

dy(:)=[dy1 dy2 dy3];

end

end

A.4   Combustor

A.4.1   Combustor attached flow

function

ALLcATT1=combATT(ALLis,gamma,R,x4,A3,D,deg,N,speName,speMW,v,vr,FAu)

%{

global M3

global gamma

global A3

global D

global dAdx

global dTtdx

global Npts

global T3

global P3

global rho3

```matlab
global R

global h

global x3

global x4

global T

global x

%}


%% combustion:


x3=0;

%x4=.8;

T3 = ALLis(end,4);

P3 = ALLis(end,3);

rho3=P3/R/T3;


M3=ALLis(end,2);


nmax=.95;

Lmax=.2;%in m


Npts=50;

h=(x4-x3)/Npts; % step size
```

```
    x = x3:h:x4;

    comb=combust(P3,T3,M3,rho3,A3,gamma,FAu,speName,N,speMW,v,vr,nmax,Lmax,x3
,x4,h);

    x=comb(:,1);

    T=comb(:,end);


    ALLcATT1=isoBur(x,T);

    ALLcATT1(:,2);


    sIS=size(ALLcATT1);
        for i=1:sIS(1)
            if ALLcATT1(i,2)<=1
                figure
                plot(ALLcATT1(:,1),ALLcATT1(:,2), 'linewidth', 1.5); hold on;
                plot(ALLcATT1(:,1),ALLcATT1(:,3)/P3, 'linewidth', 1.5); hold on;
                plot(ALLcATT1(:,1),ALLcATT1(:,4)/T3, 'linewidth', 1.5); hold on;
                plot(ALLcATT1(:,1),ALLcATT1(:,5)/rho3, 'linewidth', 1.5);
                legend("M(x)","P(x)/P3","T(x)/T3","\rho (x)/\rho_3");
                title("Thermal Choke at the Combustor")
                break
            end
        end
```

```matlab
function All=isoBur(x,T)

%{

global M3

global gamma

global A3

global D

global dAdx

global dTtdx

global Npts

global T3

global P3

global rho3

global R

global h

global x3

global x4

%global x

%global T

%}


%% Isolator parameters:


%stagnation properties:
```

```matlab
Tst3=T3*(1+(gamma-1)*(M3^2)/2);

Pst3=P3*(Tst3/T3)^(gamma/(gamma-1));

% Initializing

M= zeros(1,length(x));

Tst= zeros(1,length(x));

A= zeros(1,length(x));

P= zeros(1,length(x));

Pst= zeros(1,length(x));

rho= zeros(1,length(x));

TlT=log(T');

dlTdx=zeros(1,length(x));

dTtdx=zeros(1,length(x));

dAdx=zeros(1,length(x));


for i=1:(length(x)-1)

    dlTdx(i)=(TlT(i+1)-TlT(i))/h;

end


for i=1:(length(x))

    %dAdx(i)=h*log(((D+2*tand(deg)*(x(i)-x(1)))+2*tand(deg)*h)/(D+2*tand(deg)*(x(i)-
x(1)))));

    dAdx(i)=log(((D+2*tand(deg)*(x(i)-x(1)))+2*tand(deg)*h)/(D+2*tand(deg)*(x(i)-
x(1)))))/h;
```

```
end


%initializing

M(1) = M3; % redo with other choices here.

Tst(1)=Tst3;

T(1)=T3;

A(1)=A3;

P(1)=P3;

Pst(1)=Pst3;

rho(1)=rho3;


for i=1:(length(x)-1)

    %dMdx = @(x,M) M*2*((1+((gamma-
1)*(M^2)/2))^2)*(((1+gamma*(M^2))*dlTdx(i)/2)-dAdx)/(1-(M^2))/((2*((1+((gamma-
1)*(M^2)/2))))-((1+gamma*(M^2))*(gamma-1)*(M^2)*((1+((gamma-1)*(M^2)/2)))/(1-M^2)));

        K=@(M) M.*(1+((gamma-1).*(M.^2)/2))/(1-(M.^2));

        %KK=@(M) 1-(K(M).*(gamma-1).*M.*(1+gamma.*(M^2))./(1+((gamma-
1)*(M^2)/2))/2);

        %dMdx = @(x,M) K(M).*(-dAdx(i)+((1+gamma*(M^2))*dlTdx(i)/2))./KK(M);

        KK=@(M) 1-((M^2)*(gamma-1)*(1+(gamma*(M^2)))/2/(1-M^2));

        dMdx = @(x,M) K(M).*(-dAdx(i)+((1+gamma*(M^2))*dlTdx(i)/2))./KK(M);

        k_1 = dMdx(x(i),M(i));
```

129

```
        k_2 = dMdx(x(i)+0.5*h,M(i)+0.5*h*k_1);

        k_3 = dMdx((x(i)+0.5*h),(M(i)+0.5*h*k_2));

        k_4 = dMdx((x(i)+h),(M(i)+k_3*h));

        M(i+1) = double(M(i) + h*(k_1+2*k_2+2*k_3+k_4)/6);  % main equation


        %UTA

        A(i+1)=A(i)+h*2*.1*tand(deg);


        Tst(i+1)=T(i+1)*(T3*(1+((gamma-1)*(M3^2)/2))/Tst3/(1+((gamma-
1)*(M(i+1)^2)/2))^-1);

        P(i+1)=P3*A3*M3*sqrt(T(i+1)/T3)/A(i+1)/M(i+1);

        Pst(i+1)=Pst3*P(i+1)*((Tst(i+1)*T3/Tst3/T(i+1))^(gamma/(gamma-1)))/P(i+1);

        rho(i+1)=P(i+1)/R/T(i+1);


    end


    All=[x M' P' T rho' Pst'/Pst3 Tst'/Tst3 A'/A3];



    end



    end
```

A.4.2   Combustor with separation

```
function
ALLcSEP1=combSEP(ALLcATT1,ALLsep,Pcmax,index_cmax,gamma,R,x4,A3,D,deg,N,speN
ame,speMW,v,vr,FAu)

    x3=0;

    x=ALLcATT1(:,1);

    %New Entry Characteristics:

    M3=ALLsep(end,2);

    P3=Pcmax;

    T3=ALLsep(end,4);

    rho3=ALLsep(end,3);

    %ind=index_cmax;


    %Combustion revaluted

    nmax=.95;

    Lmax=.2;%in m

    Npts=50;

    h=(x4-x3)/Npts; % step size

    comb=combust(P3,T3,M3,rho3,A3,gamma,FAu,speName,N,speMW,v,vr,nmax,Lmax,x3
,x4,h);

    T=comb(:,end);


    sep=BurSep(x,T,length(x),Pcmax);
```

```matlab
    for i=1:index_cmax

        ALLcATT1(i,3)=sep(i,2);

    end



    for i=1:length(x)

        ALLcATT1(i,2)=sep(i,1);

        ALLcATT1(i,4)=T(i);

        ALLcATT1(i,5)=sep(i,2)/R/T(i);

    end

    ALLcSEP1=[ALLcATT1(:,1) ALLcATT1(:,2) ALLcATT1(:,3) ALLcATT1(:,4)

ALLcATT1(:,5) ALLcATT1(:,end)];

    sIS=size(ALLcSEP1);

        for i=1:sIS(1)

          if ALLcSEP1(i,2)<=1

            figure

            plot(ALLcSEP1(:,1),ALLcSEP1(:,2), 'linewidth', 1.5); hold on;

            plot(ALLcSEP1(:,1),ALLcSEP1(:,3)/P3, 'linewidth', 1.5); hold on;

            plot(ALLcSEP1(:,1),ALLcSEP1(:,4)/T3, 'linewidth', 1.5); hold on;

            plot(ALLcSEP1(:,1),ALLcSEP1(:,5)/rho3, 'linewidth', 1.5);

            legend("M(x)","P(x)/P3","T(x)/T3","\rho (x)/\rho_3");

            title("Thermal Choke at the Combustor Due to Separation")
```

```
            break

        end

    end


function All=BurSep(x,T,ind,Pcmax)


%stagnation properties:

Tst3=T3*(1+(gamma-1)*(M3^2)/2);

% Initializing

M= zeros(1,ind);

Tst= zeros(1,ind);

P= zeros(1,ind);

rho= zeros(1,ind);

TlT=log(T');

dlTdx=zeros(1,ind);

%dTtdx=zeros(1,ind);

%dAdx=zeros(1,ind);



for i=1:ind-1

    dlTdx(i)=(TlT(i+1)-TlT(i))/h;

end
```

```matlab
%UTA

%for i=2:(length(x)-1)

    %dAdx(i+1)=2*tand(1.72)/(D+2*tand(1.72)*(x(i)-x(1)));

%end

for i=1:(zeros(1,ind))

    dAdx(i)=h*log(((D+2*tand(deg)*(x(i)-x(1)))+2*tand(deg)*h)/(D+2*tand(edg)*(x(i)-
x(1)))));


end %MIT


%initializing

M(1) = M3; % redo with other choices here.

Tst(1)=Tst3;

T(1)=T3;

P(1)=Pcmax;

rho(1)=rho3;


for i=1:(ind-1)

    P(i+1)=Pcmax;


    %dMdx = @(x,M) -M.*gamma*R*dlTdx(i);

    dMdx = @(x,M) -M*dlTdx(i)/2;

    k_1 = dMdx(x(i),M(i));
```

134

```
        k_2 = dMdx(x(i)+0.5*h,M(i)+0.5*h*k_1);

        k_3 = dMdx((x(i)+0.5*h),(M(i)+0.5*h*k_2));

        k_4 = dMdx((x(i)+h),(M(i)+k_3*h));

        M(i+1) = M(i) + h*(k_1+2*k_2+2*k_3+k_4)/6;  % main equation


        %UTA

        Tst(i+1)=T(i+1)*(T3*(1+((gamma-1)*(M3^2)/2))/Tst3/(1+((gamma-

1)*(M(i+1)^2)/2))^-1);

        rho(i+1)=P(i+1)/R/T(i+1);


    end


    All=[M' P' rho' Tst'/Tst3];



end


end
```